Acta Biomaterialia 115 (2020) 299–316

Contents lists available at ScienceDirect

Acta Biomaterialia

journal homepage: www.elsevier.com/locate/actbio

Full length article

How cosmetic tightening products modulate the biomechanics and morphology of human skin

M. Pensalfini[a,b,*], M. Rotach[a], R. Hopf[a,c], A. Bielicki[d], R. Santoprete[d,*], E. Mazza[a,c,*]

[a] Institute for Mechanical Systems, Department of Mechanical and Process Engineering, ETH Zurich, Leonhardstrasse 21, Zurich 8092, Switzerland
[b] Laboratori de Càlcul Numèric, Universitat Politècnica de Catalunya-BarcelonaTech, Carrer de Jordi Girona 1-3, Barcelona 08034, Spain
[c] Empa, Swiss Federal Laboratories for Materials Science and Technology, Überlandstrasse 129, Dübendorf 8600, Switzerland
[d] L'Oréal Research & Innovation, Avenue Eugène Schueller 1, Aulnay-sous-Bois 93601, France

ARTICLE INFO

Article history:
Received 24 April 2020
Revised 18 August 2020
Accepted 18 August 2020
Available online 25 August 2020

Keywords:
Skin tightening
Soft tissue biomechanics
Material characterization
Constitutive modeling
Mechanobiology

ABSTRACT

The active and passive mechanical behavior of a cosmetic tightening product for skin anti-aging is investigated based on a wide range of *in vivo* and *in vitro* measurements. The experimental data are used to inform a numerical model of the attained cosmetic effect, which is then implemented in a commercial finite-element framework and used to analyze the mechanisms that regulate the biomechanical interaction between the native tissue and the tightening film. Such a film reduces wrinkles and enhances skin consistency by increasing its stiffness by 48-107% and reducing inelastic, non-recoverable deformations (−47%). The substrate deformability influences both the extent of tightening and the reduction of wrinkle amplitude. The present findings allow, for the first time, to rationalize the mechanisms of action of cosmetic products with a tightening action and provide quantitative evidence for further optimization of this fascinating class of biomaterials.

1. Introduction

As we are born, become adults, and then grow older, our body characteristics evolve and adapt continuously in response to internal and external stimuli. These processes originate at the subcellular scale and ultimately impact the function, shape, consistency, and appearance of our tissues and organs. Skin provides clear and visible evidence of these changes, looking silky and turgid at young age and then progressively marked by multiple signs of aging, such as wrinkle formation and tissue sagging.

Most age-induced skin alterations result from a combination of endogenous (*e.g.* gene mutations, cellular metabolism, and hormonal changes) and exogeneous factors (*e.g.* chemicals, toxins, pollutants, radiations such as the UV light, and mechanical insults) [1]. These alterations commonly affect the epidermal thickness [1,2], structure, and pigmentation [2], as well as the morphology and microstructure of deeper structures. For instance, fibrillin depletion and reduced expression of collagen type VII have been reported in the dermo-epidermal junction of aged tissues [1], possibly contributing to wrinkle formation [3]. Moreover, the mid and deep dermal layer of sun-exposed aged skin have been shown to feature abnormal elastic fiber accumulation (solar elastosis) [1], as well as sparser collagen distribution [4] and reduced collagen type I content [5]. Conversely, sun-protected aged skin displays an atrophic extracellular matrix [1], decreased cellularity (especially in terms of fibroblasts) [6,7], and fewer collagen and elastic fibers [8,9]. These changes result in visible macroscopic features characterizing the aged skin phenotype, such as reduced thickness, dryness, some loss of elasticity [6,10], and fine wrinkling for sun-protected areas, as well as laxity, roughness, irregular pigmentation, increased fragility, and deeper wrinkling in the photodamaged tissue [1]. The impact of skin aging on our lives widely exceeds its direct physiological consequences and may result in severe psychosocial distress [11], thus explaining the growing attention to maintaining a youthful and healthy skin appearance through the use of cosmetic products.

To counteract the visible hallmarks of skin aging, cosmetic industries have been striving to restore the tissue's youthful appearance through several products. A class of materials, characterized by the ability to induce significant skin tightening upon curing, has been gaining increasing attention as a promising solution to counteract the signs of aging by forming an invisible thin film that smears out superficial imperfections, mitigates wrinkles, and

* Corresponding authors.
E-mail addresses: pensalfini@imes.mavt.ethz.ch (M. Pensalfini), hopf@imes.mavt.ethz.ch (R. Hopf), ABIELICKI@rd.loreal.com (A. Bielicki), RSANTOPRETE@rd.loreal.com (R. Santoprete), mazza@imes.mavt.ethz.ch (E. Mazza).

https://doi.org/10.1016/j.actbio.2020.08.027

enhances the skin tone (see scientific publications [12–15] and numerous patents, *e.g.* [16–18]). For these biomaterials, the curing process that follows cosmetic application induces a volumetric contraction within the span of a few minutes, which results in durable skin tightening – usually lasting for several hours – and visible reduction of surface irregularities such as superficial wrinkles [12]. Indeed, Yu *et al.* [12] reported macroscopic shape correction and skin wrinkle alleviation for subjects with severe bags in the lower lid region, in line with similar findings by De Mul *et al.* for the cheek [14]. However, the effects in terms of skin apparent stiffness seem to be quite variable and possibly dependent on the specific product formulation: while Jachowicz *et al.* [13] reported a marked increase – ranging from 23% to 110% – in the equivalent elastic modulus measured *in vivo* after application of several cosmetic tightening products, this change was much more modest (4-11%) in the study by De Mul *et al.* [14] and followed the opposite trend according to Yu *et al.* [12]. In fact, these authors measured enhanced tissue deformability, besides enhanced skin elasticity (tissue return upon unloading), increased hygrometric conductance, and decreased moisture loss towards the environment.

Despite growing evidence of the effectiveness of tightening products in controlling the biomechanics and morphology of the skin *in vivo*, knowledge of their mechanical behavior is quite limited and the comprehension of the mechanical processes that regulate the interaction with the underlying native tissue remains at a qualitative level. This hinders the understanding and the possible optimization of the capabilities of these cosmetic materials. Likewise, the observation that surface wrinkles are alleviated under a contractile action [12,15] is particularly intriguing in light of the ubiquitous evidence that compression of a mechanically-graded material – such as the skin – may result in the formation or amplification of wrinkling instabilities [19–22]. In this context, the present work is concerned with the biophysical mechanisms determining the cosmetic effects obtained through application of tightening products on skin *in vivo*. Dedicated experimental protocols were developed to quantify the contractile behavior and the deformability of the studied biomaterial, providing essential data to inform a numerical model of its cosmetic outcome. This allowed rationalizing the mechanisms underlying native tissue tightening and reduction of surface imperfections by action of a film that shrinks upon curing, as well as investigating the corresponding role of several cosmetic application parameters. Specifically, the product's contractile action, its stiffness, and the substrate deformability are identified as key elements towards controlling the extent of tissue tightening and wrinkle reduction. While the analysis presented here is performed with reference to a specific product formulation, it provides insights with broad relevance for the rational design of soft active materials that aim to modulate the biomechanical and morphological features of human skin. Ultimately, we envision application of our results and numerical model to inform the development of biomaterials, which are able to reduce the appearance of the signs of skin aging.

2. Materials and methods

2.1. Characterization of the in vivo *biomechanical effects of the tightening product*

2.1.1. Subject recruitment and application of the tightening product

To quantify the effects determined *in vivo* by the application of the tightening product, 24 healthy women with a Body Mass Index (BMI) in the range of 20-28 were recruited; their age was comprised between 18 and 71 years (Fig. 1a). All volunteers gave their written informed consent before enrollment. For each subject, a 3×3 cm^2 area was identified on the lower part of the left cheek by marking its periphery with 8 ink dots (Fig. 1b). These served as fiducial points both for the application of the tightening product and for strain reconstruction. A standardized volume (220 µl) of cosmetic material was deposited on the skin surface using a syringe and rapidly spread to obtain a uniform layer of approximately 250 µm thickness, which was let cure for 30 min. The volunteer had to maintain a neutral facial expression and refrain from speaking, touching or rubbing the cosmetic film throughout the curing process.

The study was conducted in France according to the current local regulatory requirements (Decree 2017-884 of May 9th, 2017). The protocol was developed and conducted in compliance with the ethical principles adopted by the 18th World Medical Congress in Helsinki [23], and according to the guidelines issued by GCP (Good Clinical Practice) [24].

2.1.2. Quantification of tightening product contraction in vivo

Using a DermaTop-HE acquisition system (EOTech SA, Marcoussi, France), which provided a resolution of 30 µm/pixel, calibrated images of each subject's cheek were acquired before and after application of the product, at the time points indicated in Table 1. The image sequences were used to determine the skin areal strain induced by the cosmetic application. To this end, a custom-written Python code (Python Software Foundation, Wilmington, Germany) based on [25] allowed identifying the location of the 8 ink dots, from which the deformation gradient tensors corresponding to the observed skin deformation at each measurement time point were estimated using least-square error minimization. Hence, the principal strains, ε_1 and ε_2, could be computed and the areal strain was obtained as: $\varepsilon_{\text{Area}} = (\varepsilon_1 + 1)\cdot(\varepsilon_2 + 1) - 1$. Note that the product's contractile behavior leads to negative values for ε_1 and ε_2.

2.1.3. Quantification of skin biomechanical changes induced by the tightening product

Before and after 30 min of cosmetic film curing, the biomechanical characteristics of the skin within the region of application were assessed by adapting a previously-defined suction-based measurement protocol [26,27]. Most importantly, a custom-made headrest was employed to enhance measurement accuracy. Measurements were performed with two different Cutometer® probe openings (2 mm and 8 mm, Courage+Khazaka electronic GmbH, Cologne, Germany) and two different loading histories (4 protocols in total, *cf.* Fig. 1c) to characterize the elasto-viscoplastic properties of the superficial layers (cutis) and deeper tissues (subcutis). The maximum pressure for the rapid (step) loading with the 8 mm suction probe was here set to 66 mbar to ensure that the maximum skin deformation did not exceed the Cutometer® measurement range; additional details on the method and loading protocols are provided in [27]. The absence of localized fissures in the film was verified visually at the time points indicated in Table 1. This was deemed sufficient based on preliminary investigations, which indicated the emergence of a characteristic white coloring (not present in these experiments) in the fracturing film regions. Note that the critical tensile strain for the cosmetic material (data not shown) was at least one order of magnitude larger than the typical deformations induced by the suction measurements.

Comparison of the skin characteristics before and after application of the cosmetic product was based on the entire measured curves as well as on selected scalar parameters; these were obtained by averaging the measurement replicates that were available for each subject. Specifically, the maximum elevation (R0) in both the step and ramp loading protocols was used to obtain information on tissue stiffness, and the ratio R3/R0 between the residual elevation upon full unloading (R3) and the peak elevation in ramp protocols provided information on the amount of non-recoverable tissue deformation (dissipative behavior).

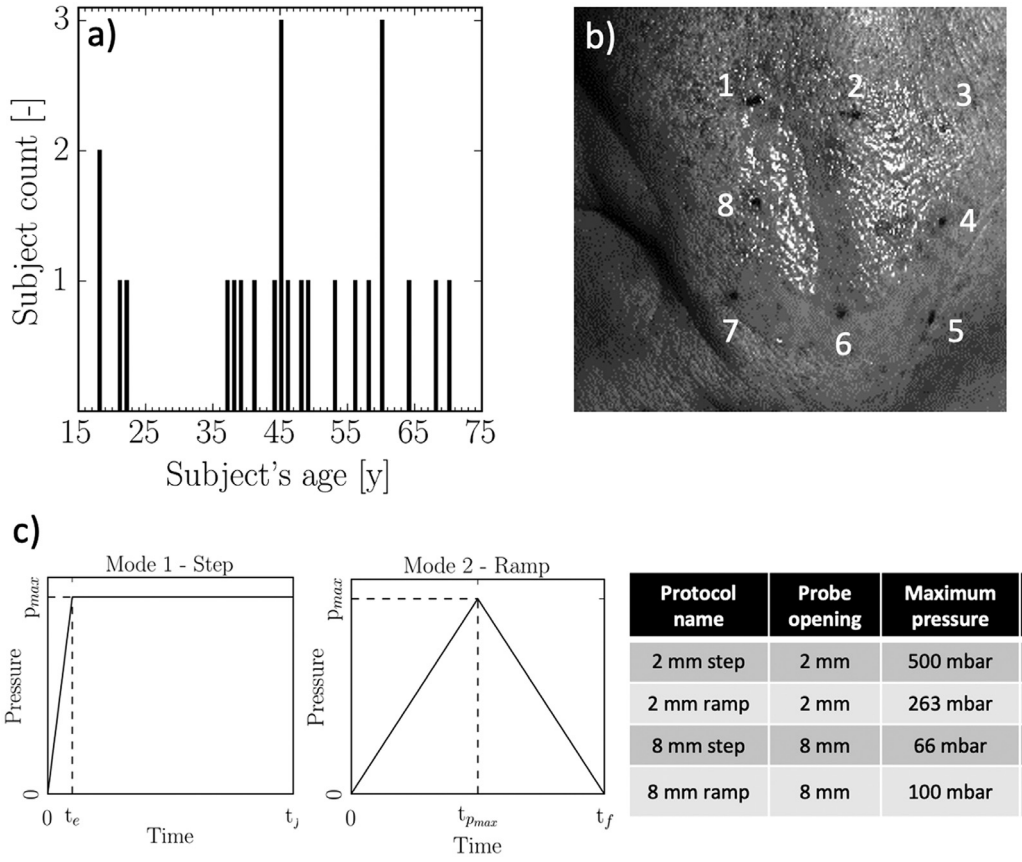

Protocol name	Probe opening	Maximum pressure	Loading time
2 mm step	2 mm	500 mbar	0.1 s
2 mm ramp	2 mm	263 mbar	15.0 s
8 mm step	8 mm	66 mbar	0.1 s
8 mm ramp	8 mm	100 mbar	10.0 s

Fig. 1. Summary of the *in vivo* experimental campaign conducted to quantify the extent of skin tightening induced by 30 min of cosmetic film application. (a) Demographics of the recruited volunteers. (b) Representative DermaTOP-HE image of the film-covered cheek, showing the 8 ink dots used for quantification of the areal contraction. The visible translucency of the cosmetic product is associated with the early time point corresponding to the displayed image and rapidly disappears with curing. (c) Schematic representation of the suction loading profiles and corresponding protocol details.

Table 1
Summary of measurement time points for quantification of the tightening product's contractile action *in vivo*.

Time [min]	0 (no film)	1	5	6	7	8	9	10	11	12	13	14	15	20	25	30

2.2. In vitro *characterization of the cosmetic film mechanical behavior*

To quantify the mechanical characteristics of the tightening product when applied on substrates of controlled properties, experiments involving cosmetic film application and curing *in vitro* were performed. As schematically shown in Fig. 2a, the contraction of the tightening product was expected to be directly influenced by the stiffness of the substrate (assuming perfect adhesion), which had to be progressively deformed to accommodate the volume change of the curing film. Thus, two different synthetic materials were used to obtain suitable substrates. The silicone-based elastomer DOWSIL™ CY 52-276 Gel (Dow Chemical Company, Midland, MI, USA), produced using a 1:1 ratio of A:B components and characterized by a Young's modulus of (6.6±0.5) kPa (see Supplementary Material), represented a substrate whose deformability widely exceeds that of human skin. On the other hand, 510 μm-thick sheets of the room temperature vulcanized (RTV) elastomer SMI G/G 0.020″ (Specialty Manufacturing Inc., Saginaw, MI, USA), which has a Young's modulus of 1.5 MPa [28], provided a substrate capable of significantly restraining the cosmetic film contraction without fully impairing it. Based on literature data [29,30], the constraining action of human skin was expected to fall between that of the two chosen substrates (Fig. 2a).

2.2.1. Quantification of the product contractile action on DOWSIL™ CY 52-276 Gel

To provide a flat surface for cosmetic application while minimally influencing the in-plane contractile behavior of the tightening product, substrates of DOWSIL™ CY 52-276 Gel with a thickness of 7 mm and a diameter of 55 mm were manufactured according to the procedure described in the Supplementary Material. Importantly, the substrates featured a 1 mm top layer enriched with colored microspheres, which provided fiducial points to reconstruct the deformation field resulting from the contraction of the cosmetic film (Fig. 2b). The product was applied by depositing a small amount on the center of the substrate and spreading it uniformly over a circular area of about 15 mm diameter using the cosmetic application tool shown in Fig. 2a. The ability to control the cured film thickness using such tool was verified in preliminary experiments (*cf.* Supplementary Material), which yielded values of (102.2±3.4) μm. After spreading the product, the substrate was immediately placed upside-down under a CCD camera (Pike F-100B; Allied Vision Technologies GmbH, Stadtroda, Germany) equipped with a 0.25× telecentric lens allowing for a 30×30 mm^2 field of view at 0.03 mm/pixel (NT55-349; Edmund Optics GmbH, Karlsruhe, Germany), and monitored for a period of about 11 h at room temperature. Observing the colored particles through the transparent DOWSIL™ CY 52-276 Gel substrate (Fig. 2b) allowed the displacement of fiducial points located along

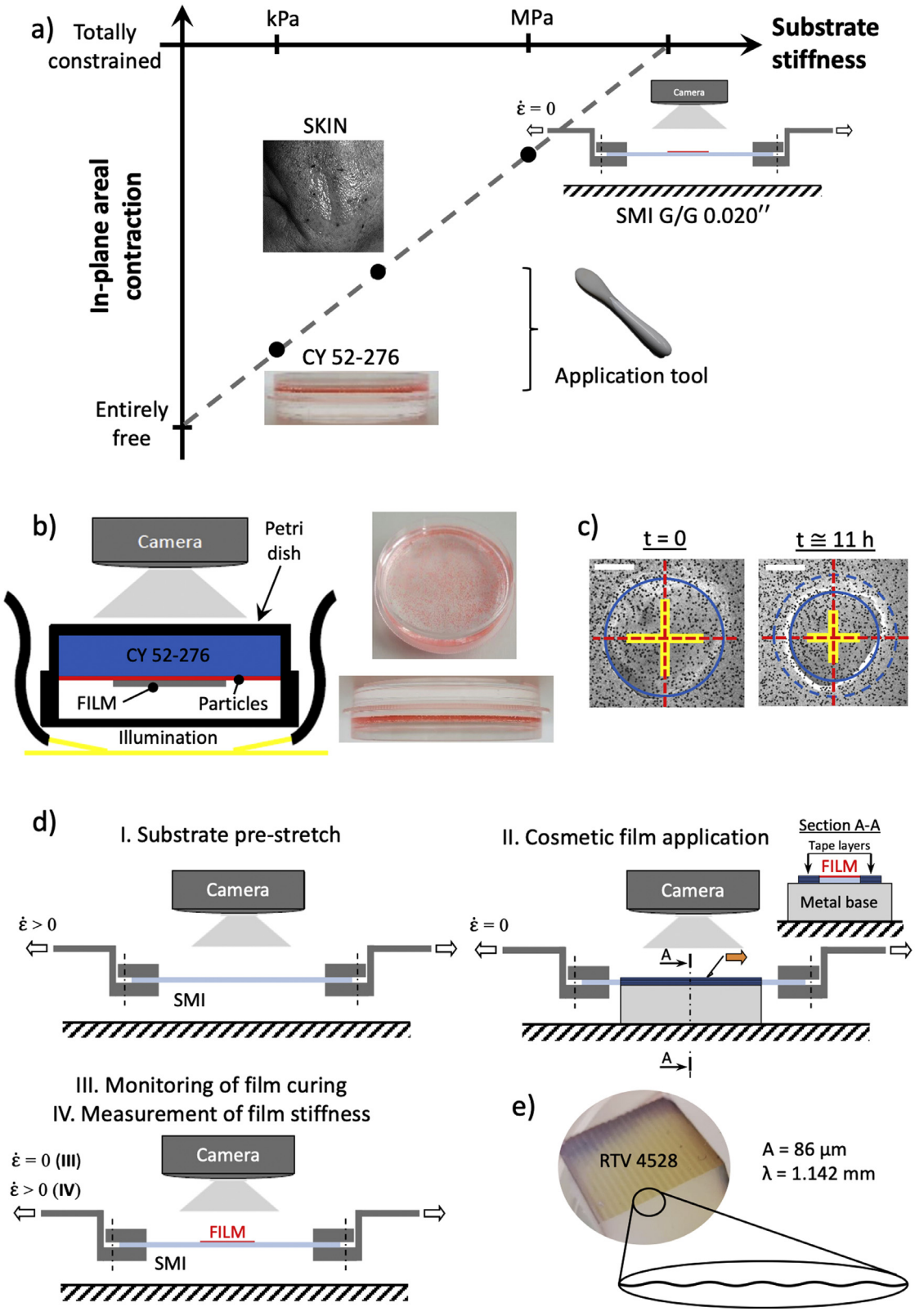

Fig. 2. Summary of the experimental campaign conducted *in vitro* to characterize the mechanical behavior of the tightening product by deposition on substrates of known geometry and mechanical properties. (a) Schematic of the expected relationship between the substrate stiffness and the extent of film contraction, which constituted the rationale for the experimental campaign. (b) Experimental method for the application on DOWSIL™ CY 52-276 Gel, allowing the film contraction to be tracked thanks to the presence of pink micro-spheres in a superficial substrate layer. (c) Example of data analysis approach for the experiments on DOWSIL™ CY 52-276 Gel, showing the regions for strain quantification and the macroscopic areal contraction of the cosmetic material (scale bar: 5 mm). (d) Experimental method for the application on SMI G/G 0.020″, involving substrate preconditioning and prestretch (I), followed by film deposition (II) and curing (III), and finally extension of the SMI + Film structure in order to quantify the stiffness of the cosmetic material (IV). (e) Wrinkled substrate for application of the tightening product; the wrinkle profile is also drawn magnified for clarity. (For interpretation of the references to colors in this figure legend, the reader is referred to the web version of this article.).

two mutually-orthogonal radial lines to be tracked and used to determine the corresponding line strains in the film-covered region (yellow rectangles in Fig. 2c) according to a previously-presented optical method [25,31]. The areal strain at each measurement time point was determined from the radial strains, ε_{R_1} and ε_{R_2}, as: $\varepsilon_{Area} = (\varepsilon_{R_1} + 1) \cdot (\varepsilon_{R_2} + 1) - 1$. Due to the time needed to place the substrate under the camera, the image of the undeformed configuration was not available. Instead, deformations were determined with respect to the image corresponding to the first instant of visible film contraction (after the characteristic initial expansion described in Sections 3.1 and 3.2.1, which is visible in Fig. 5a).

2.2.2. Quantification of tightening product contraction and stiffening on SMI G/G 0.020″

To provide stronger constraints to the in-plane contractility of the cosmetic film, 510 μm-thick sheets of SMI G/G 0.020″ were purchased and cut to obtain specimens having in-plane dimensions of 60×10 mm^2 (length × width). After introducing an ink pattern for subsequent quantification of the deformation field, the specimens were clamped (gauge length: 40 mm) in a custom-built displacement-controlled multiaxial testing setup (Fig. 2d) comprising two horizontal hydraulic actuators (MTS Systems, Eden Prairie, MN, USA) with load cells calibrated for a force range of 10 N and custom-made clamps, as well as the CCD camera and telecentric lens described in Section 2.2.1. After preconditioning to 50% strain for 200 cycles at 1 Hz (Fig. 2d I), the elastomer was elongated to 24% strain (measured as nominal value obtained from clamp to clamp distance; elongation rate: 0.1 mm/s), followed by stress relaxation for 2 min. In this configuration, the setup shown in Fig. 2d II was used to spread 17 μl of tightening product on the entire width of a 15 mm-long central region of the specimen. Specifically, a metal bar supported the SMI G/G 0.020″ membrane and provided reference features (tape layers) to ensure a cosmetic film thickness of about 110 µm, while an operator homogeneously spread the product using a second bar. The film curing was monitored for a period of almost 2 h (at room temperature) by recording images of the deforming specimen and continuously acquiring the force signal provided by the load cells (Fig. 2d III). After the curing phase, some of the specimens were extended by an additional 10% (overall nominal strain: 36.4%) at a rate of 0.37 mm/s in order to quantify the stiffness of the cured film (Fig. 2d IV). Throughout the experiments, the strains in the SMI G/G 0.020″ substrate – both in the region covered by the product and that free from it – were quantified along the specimen centerline using a previously-presented optical method [25,31]. The cured film thickness was measured as described in Section 2.2.1 from slices of the entire specimen; that is, the film was not detached from the substrate.

2.2.3. Quantification of product wrinkle-alleviating action on SILBIONE® RTV 4528

To provide experimental evidence of the wrinkle alleviation associated with cosmetic application on a substrate possessing skin-like deformability, a corrugated substrate of SILBIONE® RTV 4528 (Young's modulus: 48.6 kPa [28]) with in-plane dimensions of 20×45 mm^2 (width × length) and a thickness of 14 mm was manufactured according to the procedure described in the Supplementary Material. This substrate, whose surface corrugation had periodicity λ = 1.142 mm and amplitude A ≈ 86 µm (see sketch in Fig. 2e), was uniformly covered with about 100 µl of tightening product using the application tool shown in Fig. 2a. After letting the cosmetic film cure for 3.5 h at room temperature, the specimen was cut and placed sideways under a Zeiss LSM Pascal 5 (Carl Zeiss, Oberkochen, Germany) confocal microscope equipped with an AxioCam ICc3 camera (pixel size: 3.45×3.45 μm^2) and a 5× magnification objective; this allowed quantifying the wrinkle geometry after application of the product. The Trainable Weka Segmentation plugin [32] available within ImageJ [33] was used to identify the boundaries between the cosmetic film and the substrate and between the film and the image background, which allowed the dry film thickness and final wrinkle shape to be determined.

2.3. Finite element models to clarify the mechanisms underlying skin tightening

A constitutive model of the cosmetic film action was established based on the *in vitro* experiments described in Sections 2.2.1 and 2.2.2 and implemented in Abaqus 6.14-1 (Simulia, Dassault Systèmes, Johnston, RI, USA) for use in finite-element simulations, followed by validation using both *in vitro* and *in vivo* data. This section provides details on the finite-element models used to represent each experimental condition; the constitutive model of the tightening product will be presented in Section 3.3.1 as part of the results. Note that, as cosmetic mass loss was not included in the modeling, representation of the film thickness was based on the final dry values.

2.3.1. Simulation of in vivo product application: contraction upon curing

Calculations were performed using a 3D finite-element model of the human face, which included anatomical details of bones, muscles, fat layers, and cutaneous tissues (Fig. 3a). This model was a generic one and did not specifically correspond to the facial morphology of any of the subjects. The soft tissues were modeled as quasi-incompressible Rubin-Bodner materials, allowing the full elasto-viscoplastic behavior of cutis and subcutis to be represented [34,35]. The corresponding material model coefficients (Table 2) were determined based on the average elevation-time curves experimentally measured on the bare cheek, *i.e.* prior to cosmetic product application (*cf.* Supplementary Material). The resulting long-term secant moduli (at 5% strain in uniaxial tension) were of 33.3 kPa for the cutis and 2.5 kPa for the subcutis. Further model details are provided in the Supplementary Material.

The application of a thin cosmetic film was simulated by duplicating the outermost faces of the elements corresponding to the cheek region delimited by the ink dots visible in Fig. 1b. Those faces were used to define quadrilateral shell elements with reduced integration (S4R), which were tied to the underlying cutis in order to represent the cosmetic material (Fig. 3a). As the cured film thickness *in vivo* was not measured, a value of approximately 60 μm was assumed based on the thickness reduction observed in the *in vitro* tests.

To account for the presence of gravity during the application of the tightening product *in vivo*, for this specific simulation the face model was first subjected to long term application of a gravimetric field (corresponding to the subject being in the erect position), followed by simulation of the film curing. Note, however, that the influence of gravity on the results reported in Fig. 7a is negligible, as confirmed by comparing simulations with and without gravimetric field (data not shown). The extent of product contraction at each simulation time increment was determined by quantifying the maximum and minimum in-plane strain for each shell element, computing the 'per-element' areal strain, and finally averaging these values over the entire shell representing the cosmetic film; the configuration reached after gravimetric load application was used as reference to quantify areal strains.

2.3.2. Simulation of in vivo product application: skin stiffening after curing

To simulate the apparent skin stiffening caused by the presence of a cured cosmetic film, 2D axisymmetric models of the suction experiments carried out after product application were prepared.

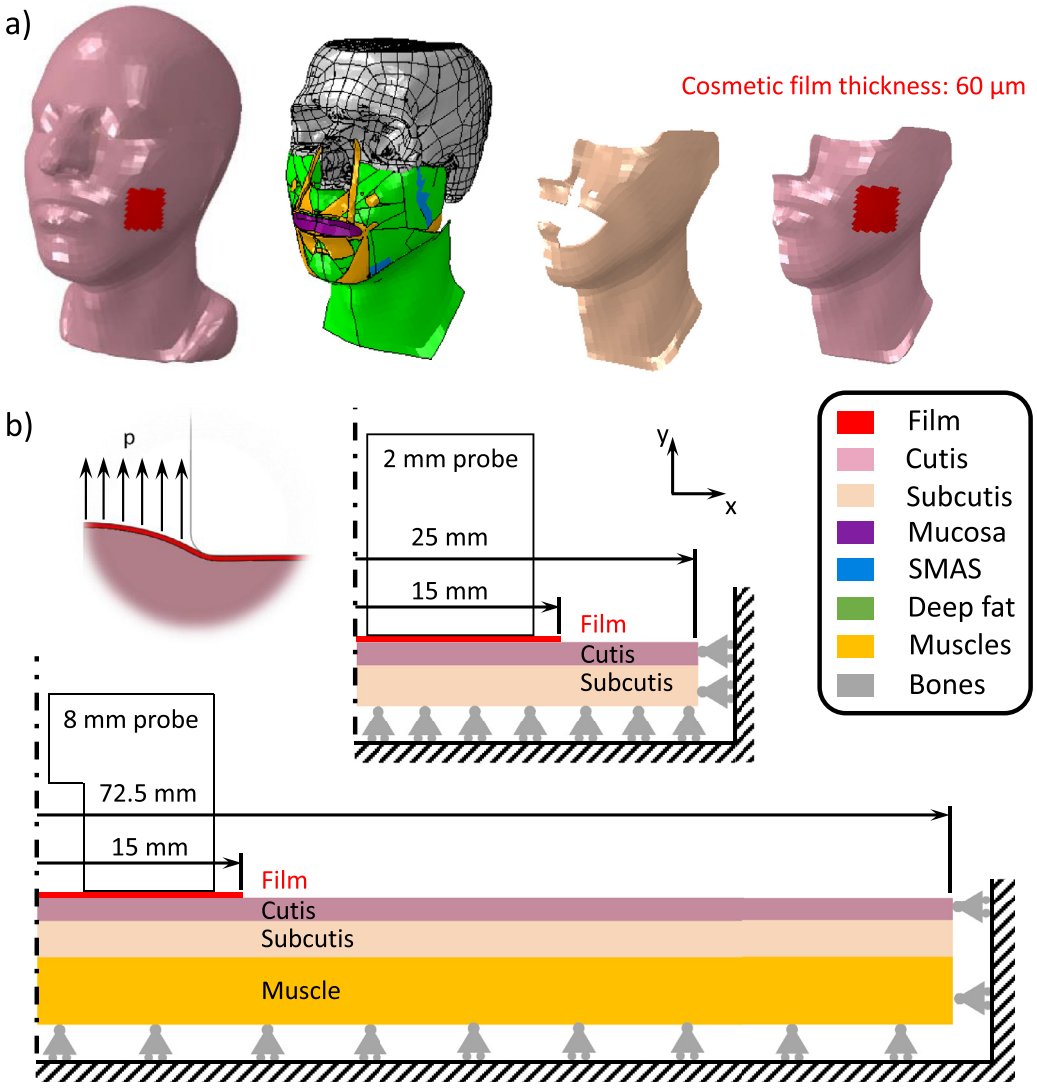

Fig. 3. Finite-element models of tightening product application *in vivo*. (a) Anatomical details of the 3D model of the human face used to simulate the cosmetic film contraction on the cheek; the region selected for cosmetic application is visible in red. (b) 2D axisymmetric models of the suction experiments employed to quantify the cosmetic-induced tissue stiffening.

Table 2
Material model coefficients adopted to describe the cutis and subcutis elasto-viscoplastic behavior according to a Rubin-Bodner constitutive formulation. The values in the top rows were determined from inverse analysis of the experimental data collected as part of the present study, while those in the bottom rows were obtained from Weickenmeier *et al.* [26].

Tissue layer	μ_0 [kPa]	q [-]	m_2 [-]	Γ_1 [Hz]	Γ_2 [-]	r_2 [-]
Cutis	52.5	28.5	0.028	1.21	72.6	6.50
Subcutis	2.94	50.2	0.21	54.1	31.2	2.55

Tissue layer	ρ [g/cm^3]	m_1 [-]	m_3 [-]	m_4 [-]	m_5[§] [-]	n [-]	r_1 [-]	r_3 [Hz]	r_4[†] [Hz]	r_5 [-]
Cutis	1.1	1000	0.0	1.0	0.972	0.5	20.0	10^{-10}	10^{-3}	1.0
Subcutis	1.0	1000	0.0	1.0	0.789	1.0	0.2	10^{-8}	10^{-3}	1.0

§ Determined as $m_5 = 1 - m_2$, *cf.* [26].
† Reduced by one order of magnitude with respect to the values considered in [26] in order to reach steady-state tissue behavior within the considered time span.

Specifically, the simulations represented curing of the product on skin for 30 min, followed by application of a suction loading according to the employed experimental protocols. This was achieved by using the models presented in [26], which were adapted by introducing a 60 μm-thick cosmetic film that was tied to the upper surface of the cutis (Fig. 3b). The thickness of the cutis, subcutis, and muscle layers was of 1.7, 3, and 5 mm, respectively [26]. The geometry and boundary conditions considered for the models are displayed in Fig. 3b; further details are provided in the Supplementary Material. Note that the layer underlying the subcutis in the 8 mm probe simulations clearly constitutes a simplification of the several tissue structures present below the skin and its material model coefficients were thus directly adopted from [26].

2.3.3. Simulation of product application on flat synthetic substrates

Finite-element models corresponding to the experiments on flat synthetic substrates (DOWSIL^{TM} CY 52-276 Gel, *cf.* Fig. 4a, and SMI G/G 0.020″, *cf.* Fig. 4b) were prepared according to the details described in the Supplementary Material. The mechanical behavior of

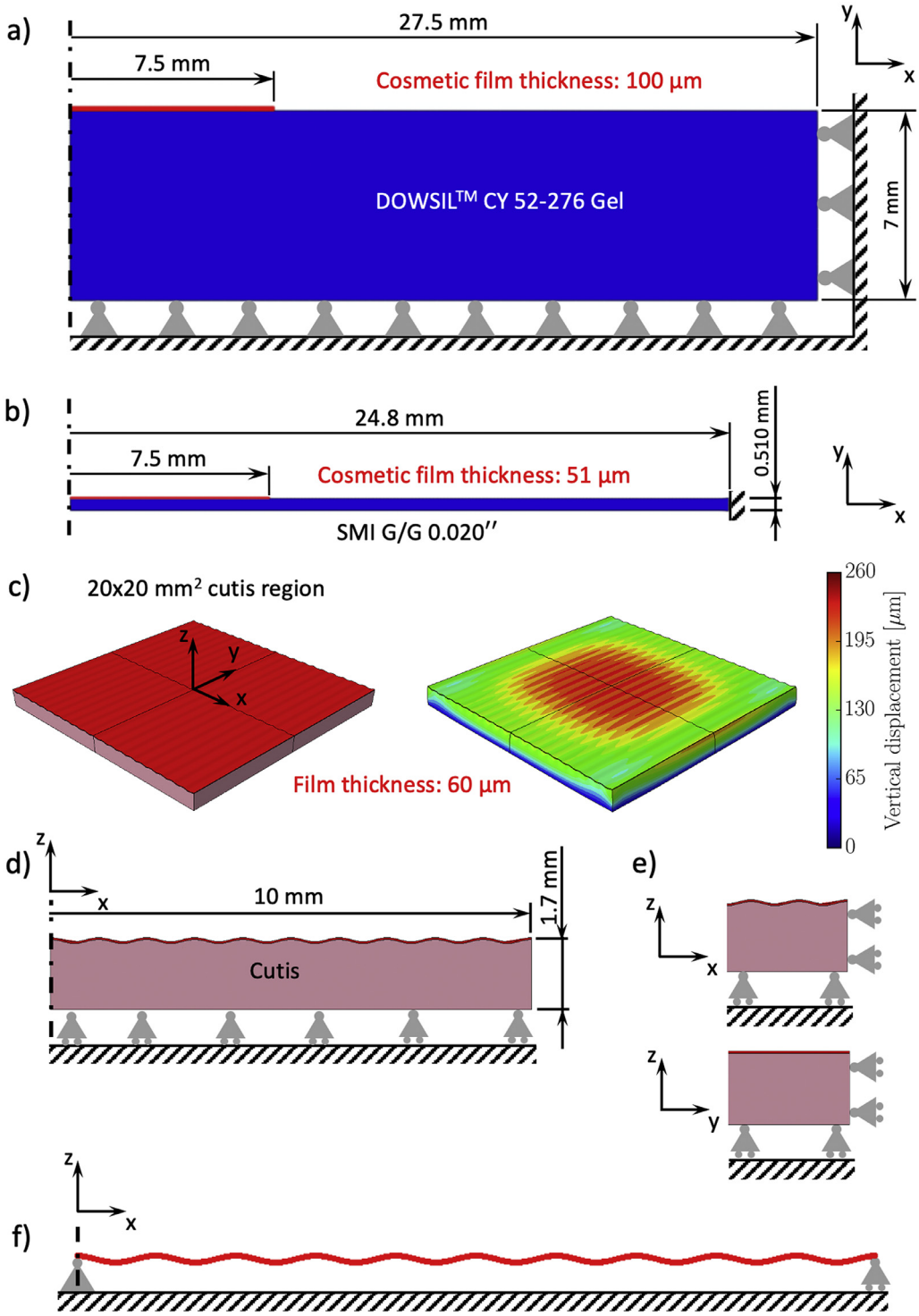

Fig. 4. Finite-element models of tightening product application on synthetic substrates and on wrinkled cutis *in silico*. (a) 2D axisymmetric model of the application on the DOWSIL™ CY 52-276 Gel substrate. (b) 2D plane stress model of the application on the SMI G/G 0.020″ membrane after the substrate has been pre-stretched. (c) 3D model of the application on a wrinkled cutis, including a representative image showing the vertical displacement field after 30 min of curing. (d) Side view (xz plane) of the wrinkled cutis, showing the boundary conditions that were applied to represent absence of skin tension. (e) Boundary conditions used to represent a level of skin tension that fully constrains the in-plane displacement. (f) Side view (xz plane) of the finite-element model of cosmetic film contraction in the absence of a substrate, showing the applied boundary conditions.

the DOWSIL™ CY 52-276 Gel was described using a 2nd order incompressible Ogden model, which was derived from [36] by scaling the values of μ_1 and μ_2 to match the mechanical response measured here by indentation (see Supplementary Material). Conversely, the behavior of SMI G/G 0.020″ was described by the 3rd order incompressible Ogden model formulation proposed in [28]. The rationale for using a purely elastic constitutive model for SMI G/G 0.020″ was the modest stress relaxation observed in the present measurements (data not shown). In order to compare the finite-element predictions with the corresponding experiments on DOWSIL™ CY 52-276 Gel, the simulated substrate radial strain, ε_R, was quantified based on the displacement of nodes that are found

within a 1 mm-thick region below the cosmetic film. The areal deformation was then determined as: $\varepsilon_{Area} = (\varepsilon_R + 1)^2 - 1$. As for the product application on SMI G/G 0.020″, the simulated longitudinal strains in the substrate were determined from the coordinates of selected nodes, which were chosen to exclude possible boundary effects at the clamps and at the transition between the SMI G/G 0.020″ regions covered by and free from the cosmetic film. The reaction force at each clamp was quantified by summing the nodal reactions arising from the applied boundary conditions (Fig. 4b). Comparison with the experiments was based on the x-component of the total force.

2.3.4. Simulation of product application on wrinkled substrates

To clarify the mechanisms underlying the wrinkle-alleviating action of skin tightening products, a 20×20 mm^2 corrugated tissue region was modeled, exploiting symmetry, according to the details provided in the Supplementary Material. The skin was modeled as a 1.7 mm-thick cutis layer [26] with material parameters chosen according to Table 2. The contribution of the very soft subcutis was represented by subjecting the bottom nodes of the cutis to boundary conditions that allowed them to slide parallel to the tissue plane, but prevented any displacements along z (Fig. 4d). Furthermore, a model preventing in-plane displacements of the skin edges was also considered in order to exaggerate the possible influence of skin tension on the extent of product contraction (Fig. 4e). In addition, the cosmetic film curing in the absence of a substrate was simulated by removing the skin elements and subjecting the film to boundary conditions corresponding to a simply supported plate (Fig. 4f). For all the above models, the amplitude and periodicity of the first wrinkle profile laying on the xz plane and closest to the yz plane were quantified and used to determine corresponding relative changes (akin to strains) with respect to the initial shape. The simulated time span for film curing was restricted to 30 min, in line with the relatively short duration of the *in vivo* experiments described in Section 2.1.

Finally, a model specifically representing the experiment described in Section 2.2.3 was also prepared in order to extend the validation of the numerical model of the studied tightening product to wrinkle-alleviating applications. The constitutive formulation for SILBIONE® RTV 4528 was based on [28] and the model exploited symmetry about the xz and yz planes. After simulating 3.5 h of film curing, the boundary condition ensuring symmetry with respect to the xz plane was released in order to represent the specimen cutting required for wrinkle shape visualization; the reached equilibrium configuration was used to measure the final wrinkle amplitude.

2.5. Statistical methods and data representation

Throughout this paper, experimental quantities are reported in terms of mean measured value and standard deviation (error bars or shadings). Statistical comparison of Cutometer® parameter values before and after application of the tightening product was based on two-sided paired *t*-tests; normality of the sample difference was confirmed by performing Shapiro-Wilk's test (*cf.* Supplementary Material). The threshold for significance was set to $p < 0.05$, and analysis was performed using the statistical module available within the SciPy Python package (Python Software Foundation, Wilmington, Germany).

3. Results

3.1. In vivo *application of the skin tightening product*

Controlled application of the product on the left cheek of 24 women consistently showed rapid contraction of the skin region that was covered by the cosmetic film, which was already measurable after 15 min from the moment of product application. After 25-30 min, a steady state was approximately reached, corresponding to an areal strain of (−9.6±2.9)% (Fig. 5a). Interestingly, the tightening product initially displayed a modest expansion in all experiments (*e.g.* time point at 1 min in Fig. 5a), which was interpreted as indicative of the moment when the curing process began.

Quantification of the tissue biomechanical response to suction loading after 30 min of product curing showed clear stiffening of the film-covered tissue region, the average maximum tissue elevation (R0) being reduced by 32.6% and 51.7% for the 2 mm step and ramp loading modes, respectively (Fig. 5b). Likewise, the average maximum elevations were reduced by 42.8% (step) and 39.2% (ramp) in the experiments performed with the 8 mm probe opening (Fig. 5c). The ramp loading protocol, which involved complete unloading of the tissue, additionally provided information on the effects of the cosmetic film on the apparent skin elasticity. The R3/R0 ratio was reduced by 47.1% for the 2 mm experiments, whereas it was only modestly affected (−6.9%) for the larger suction probe (Fig. 5d). This indicated a marked reduction in the dissipative behavior of the cutis layer when covered by the film, as opposed to a much more modest effect when also the subcutis was included in the comparison. Paired *t*-tests comparing the results before and after application of the product confirmed that all differences were significant with $p < 0.0001$, except for the one among the 8 mm R3/R0 ratios ($p = 0.248$). Taken together, these results provide evidence for a two-fold tightening action of the product on human skin, whereby contractility is combined with mechanical effects that lead to an increase in both the apparent stiffness and the reversibility of deformation (*i.e.* decreased inelastic, non-recoverable deformations).

3.2. In vitro *substrate tightening through application of a cosmetic film*

3.2.1. The substrate stiffness modulates the extent of product contraction

Application of the product on DOWSIL™ CY 52-276 Gel yielded a peak areal strain of (−13.0±1.0)%, which was reached almost completely after 2 h from the moment of cosmetic application (Fig. 6a). On the other hand, the SMI G/G 0.020″ membranes significantly limited the product's contractile ability, resulting in a longitudinal strain of (−2.4±0.5)% in the region covered by the film (Fig. 6b, red solid line and shading labeled as "SMI + Film"), and of (1.4±0.2)% in the surrounding SMI G/G 0.020″ (Fig. 6b, solid black line and grey shading labeled as "Bare SMI"). Correspondingly, the product contraction resulted in a force increase of (72.6±14.1) mN (Fig. 6c). Assuming in-plane isotropic contraction of the cosmetic layer, an areal strain of −4.7% could be estimated for the membrane region that was covered by the film. This value amounts to about ½ and ⅓ of the peak contraction reached on skin and on DOWSIL™ CY 52-276 Gel, respectively. Note that only the data measured following the initial product expansion (see, *e.g.*, Fig. 5a) are shown in Fig. 6a–c. Taken together, these results confirm the posited dependency of product contraction on the substrate stiffness (Fig. 2a), which is recapitulated in Fig. 6d and approximately follows a logarithmic relationship.

3.2.2. Mechanical characteristics of the cosmetic film after curing

The film resistance to deformation was determined by extending the film-covered SMI G/G 0.020″ specimens uniaxially, after letting the cosmetic layer cure for about 2 h. The measured force is shown in Fig. 6e (black curve and grey shading), which also indicates the force required to extend the SMI G/G 0.020″ by a corresponding amount (blue line). This was obtained analytically by

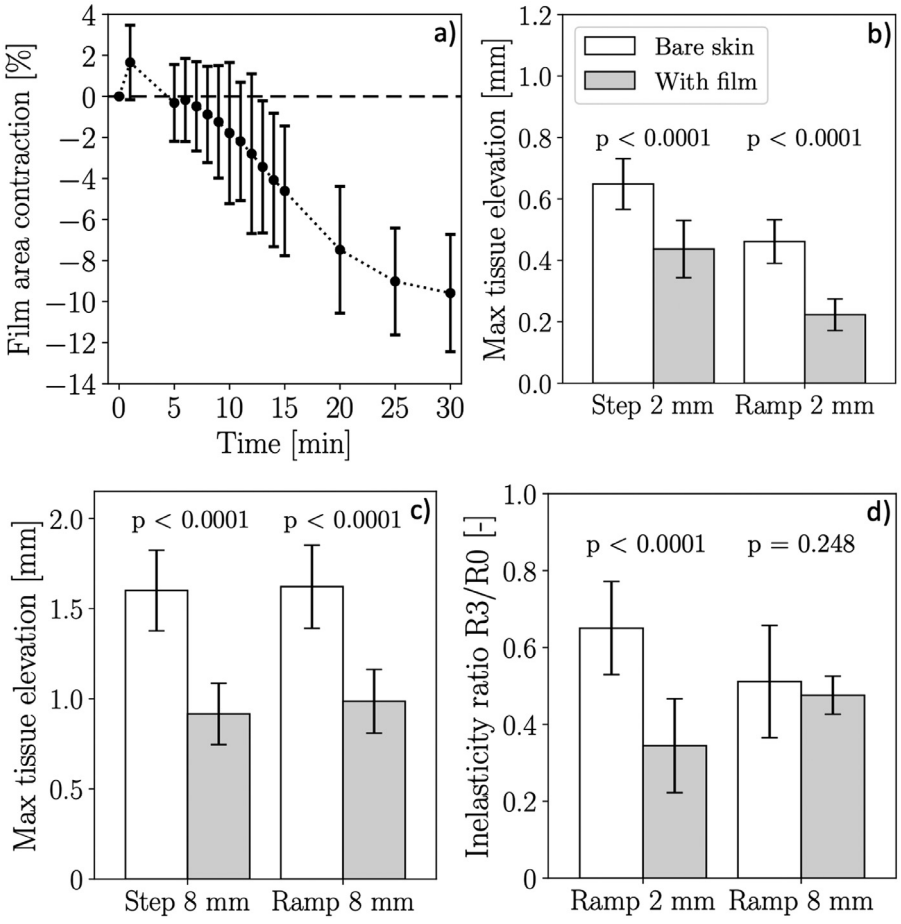

Fig. 5. Results of the *in vivo* characterization of the tightening action of the cosmetic product, as measured in the film-covered tissue region. (a) Areal contraction upon curing, showing the characteristic initial expansion (time point at 1 min), followed by rapid contraction and stabilization after 25-30 min; $n = 1$ for the time point at 0 min and $n = 24$ for every other time point. (b and c) Peak tissue elevation in 2 and 8 mm suction experiments employing a step or ramp load, showing the clear stiffening due to the presence of the cosmetic film; the differences are strongly significant ($p < 0.0001$, $n = 24$ for each displayed bar). (d) Inelasticity ratio R3/R0 for 2 and 8 mm suction experiments employing a ramp load, showing enhanced elasticity for the 2 mm probe ($p < 0.0001$) and a modest difference ($p = 0.248$) for the 8 mm one ($n = 24$ for each displayed bar).

considering uniaxial extension according to the hyperelastic material model presented in [28]. The difference between these curves identifies the net force acting on the cosmetic layer (red curve and shading). Measuring the final film thickness, which amounted to (51.4±1.3) μm, allowed determining the nominal stress-strain curve for the cured biomaterial (Fig. 6f) and the corresponding Young's modulus (first 2% strain) of (11.6±1.3) MPa.

3.3. Constitutive modeling of the product's tightening action

3.3.1. Constitutive model formulation and calibration

Aiming to rationalize the mechanical interaction between the cosmetic material and the skin, a numerical model of the product action was derived based on the *in vitro* data presented in Section 3.2. The passive deformation behavior was described by an incompressible 2nd order polynomial hyperelastic model [37], selected as the one yielding the minimum root-mean-square error with respect to the mean stress-strain curve obtained experimentally (*cf.* Supplementary Material); the model prediction is represented by a dashed line in Fig. 6f. For simplicity, the product's material model coefficients were considered to be constant during the curing process. The contraction (*i.e.* active) behavior was modeled by representing geometrical changes as if they were induced by a variation in temperature. This was obtained by attributing an isotropic thermal expansion coefficient of 1.32%/K to the product and imposing a (pseudo-) temperature variation of −6.74 K, whose time evolution directly followed the contraction kinetics shown in Fig. 6a. While the prescribed thermal difference represented the radial strain corresponding to the experimental results reported in Fig. 6a, the expansion coefficient was chosen in order to match those experiments in corresponding finite-element simulations (dashed line in Fig. 6a). The material model parameters that represent the mechanical behavior of the tightening product are summarized in Table 3. Note that the observed initial expansion (Fig. 5a) is not described by the present numerical model.

3.3.2. Numerical model validation

Both *in vitro* and *in vivo* experiments were used as benchmark for model validation. Simulation of the product application on an SMI G/G 0.020″ membrane showed an excellent ability to predict the force increase induced by the cosmetic film contraction (dashed line in Fig. 6c), and yielded strain values that fell well within the experimental standard deviation (dashed lines in Fig. 6b). Strikingly, also the simulation of the product action *in vivo* was in excellent agreement with the experiments in that it correctly captured the contraction of the film-covered cheek skin region (solid line in Fig. 7a, starting from the 1 min time point according to the modeling assumptions described in Section 3.3.1). Moreover, *in silico* application of the product on the facial skin allowed quantifying the effects on the surrounding tissues, high-

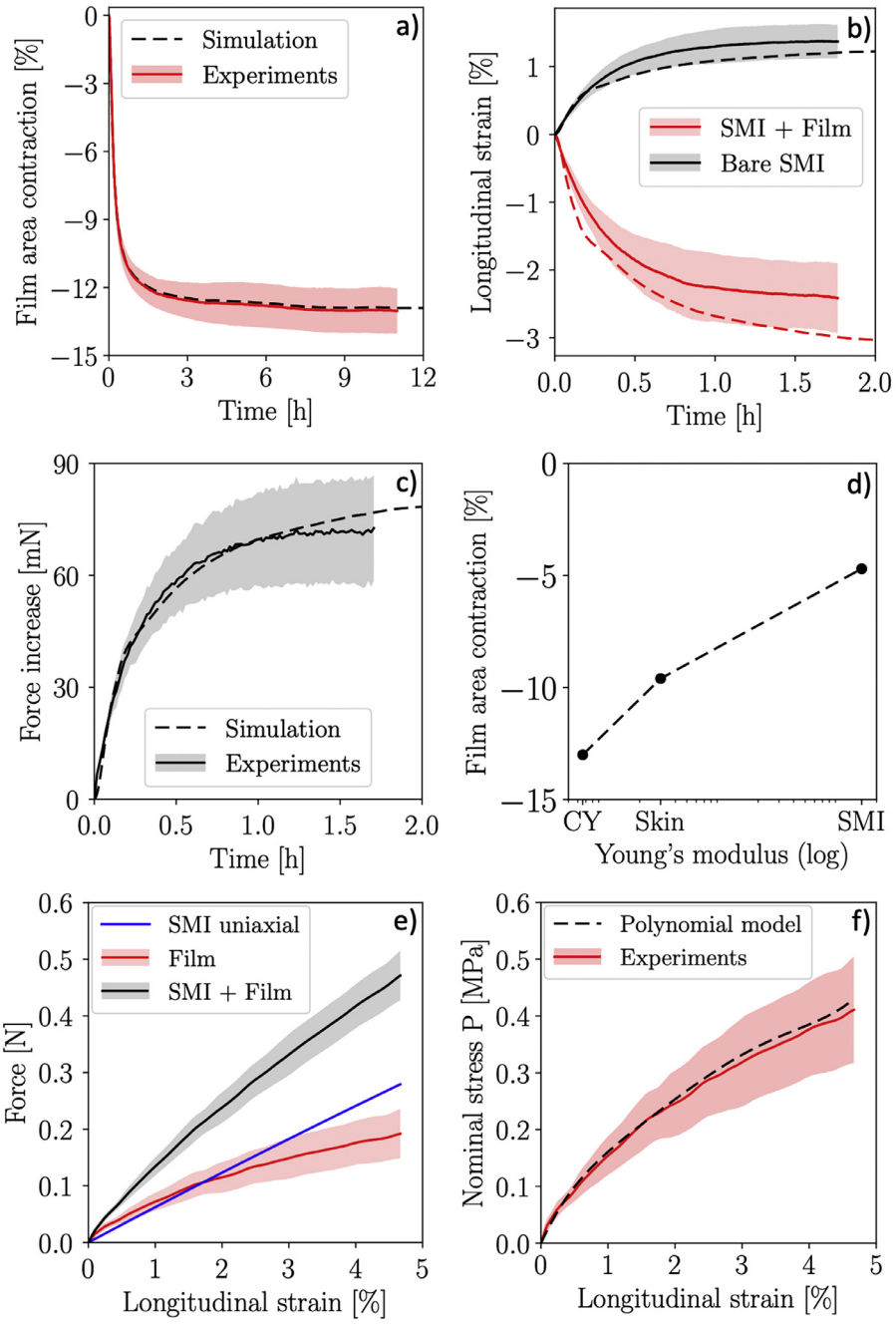

Fig. 6. Results of the *in vitro* experimental campaign conducted to characterize the mechanical behavior of the tightening product and derive a corresponding numerical model; the model predictions for each experiment are also shown as dashed lines. (a) Area contraction on the DOWSIL™ CY 52-276 Gel substrate ($n = 4$). (b) Longitudinal strains in the SMI + Film (red) and bare SMI (black) regions of the SMI G/G 0.020″ membranes ($n = 12$). (c) Force increase due to the extension of SMI G/G 0.020″ as a consequence of cosmetic film contraction ($n = 12$). (d) Relationship between the substrate stiffness and the area contraction of the tightening product. (e) Force-strain relationship obtained when extending the SMI + Film structure, showing the total force (black line and grey shading, $n = 6$), the force required to extend the SMI G/G 0.020″ membrane by a corresponding amount in a uniaxal tensile test (blue), and the resulting net force acting on the cosmetic film (red, $n = 6$). (f) Stress-strain curve for the cured film (red line and shading, n = 6) and corresponding fit using a 2nd order polynomial model (black). (For interpretation of the references to colors in this figure legend, the reader is referred to the web version of this article.).

lighting the fact that the film contraction can induce tissue displacements in the mm range – and thus skin tightening – also outside its region of application (Fig. 7b). Finally, the apparent tissue stiffening was adequately represented by the presented model for both the 2 and 8 mm probe opening experiments (dashed lines in Fig. 7c–f), despite slightly underestimating the creep behavior (Fig. 7c and e). This is most probably associated with a non-entirely elastic behavior of the cosmetic layer, which is not described by the chosen constitutive model formulation.

3.4. Mechanisms of wrinkle alleviation via tightening product application

To understand the interaction of a cosmetic layer with a corrugated substrate, the product application on a cutis featuring surface wrinkles was investigated *in silico* using the models shown in Fig. 4c-f. After 30 min of simulated curing, the wrinkle amplitude reduction in the absence of skin tension (*cf.* Fig. 4d) reached 25.5%, whereas the periodicity, λ, was only reduced by 5.9% (Fig. 8a

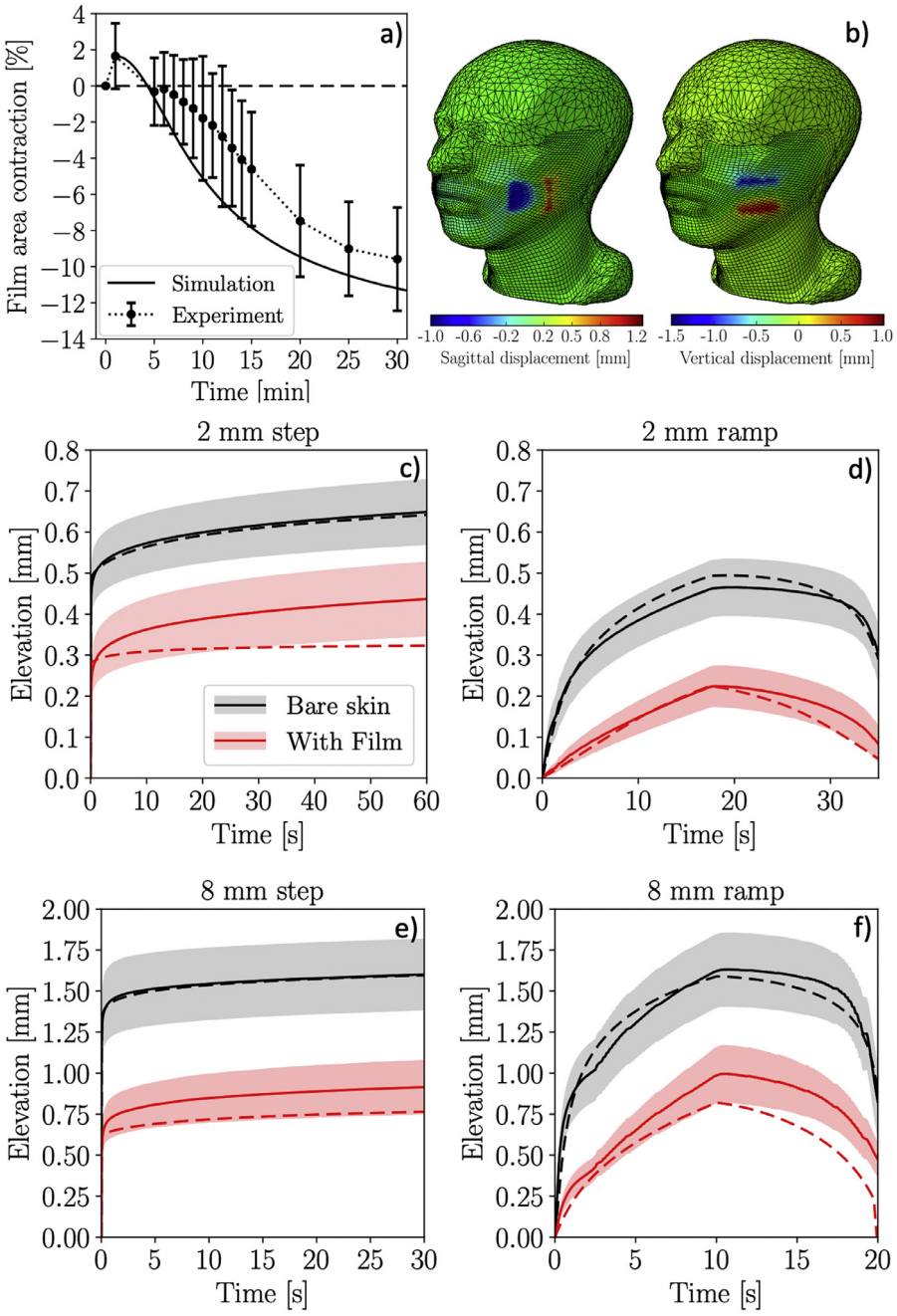

Fig. 7. Validation of numerical model against *in vivo* data of cosmetic action on the film-covered tissue region. (a) Contraction of the film-covered area as predicted by the model (black solid curve), which provides a good representation of both the extent and kinetics of contraction that were measured *in vivo* (dotted line and error bars, $n = 24$). (b) Global effect of tightening product application on the face, inducing displacements in the mm range for both the sagittal and vertical directions. (c–f) Mechanical behavior of the bare and film-covered skin as predicted by the model (dashed lines) and measured experimentally (solid lines and shadings, $n = 24$): combining the constitutive models that were determined for the cosmetic film, the cutis, and the subcutis behavior allows capturing the main mechanical features of cosmetically-treated tissues reasonably well.

and b). Conversely, simulating the contraction of the product in the absence of any substrate (*cf.* Fig. 4f) yielded a 7% reduction in both geometrical parameters (Fig. 8a and b). The clear contrast between these two conditions suggested the presence of additional phenomena at play besides the cosmetic product's volume change, which are discussed in the following. Specifically, it was hypothesized that limiting the in-plane contraction – such as when additional material is present beneath the film or around the film-covered region – may further affect the wrinkle shape and thus result in enhanced amplitude reduction, which is required to accommodate the product volume change. Indeed, when additionally limiting the skin in-plane displacement by adding boundary conditions that completely prevented the movement of the nodes at the substrate periphery (representing an idealized skin constraint, *cf.* Fig. 4e), and thus did not permit any film contraction along the x and y directions, the amplitude reduction reached 79.1%, *i.e.* the wrinkles were almost entirely flattened (Fig. 8a and b).

Finally, to verify experimentally that depositing the tightening product on a substrate may amplify the extent of wrinkle amplitude reduction with respect to the case where no substrate is present (free contraction, *cf.* Fig. 4f), a corrugated specimen made of SILBIONE® RTV 4528 was uniformly covered with a cosmetic

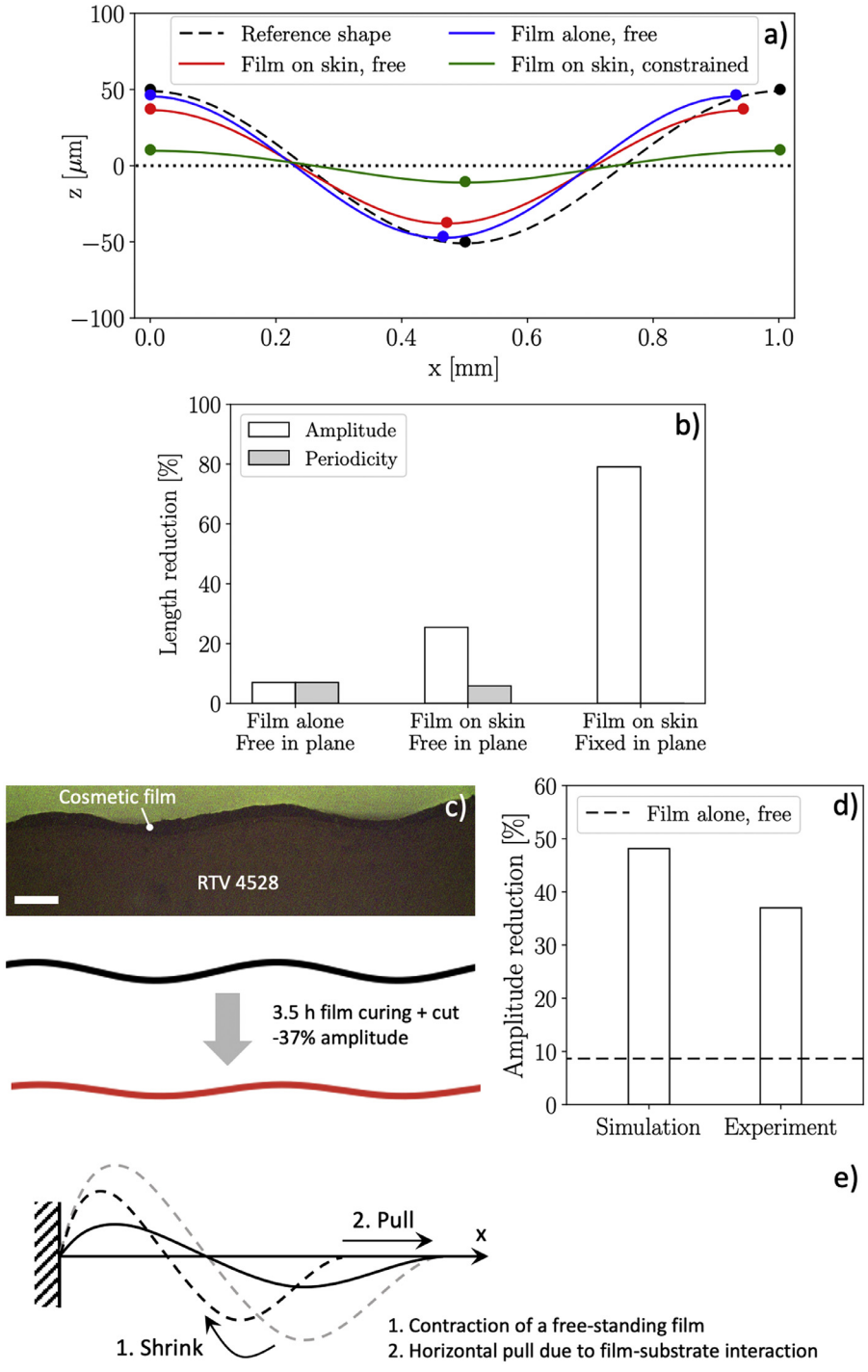

Fig. 8. Wrinkle flattening by action of a contractile cosmetic film. (a) Wrinkle shapes before the tightening product application (black dashed curve), after product curing in the absence of outer constraints (blue curve), and after application and curing on a wrinkled cutis without tension (red curve), or on a cutis with idealized peripheral constraints (green curve). (b) Amplitude and period reduction for the three described cosmetic application conditions: the wrinkle flattening is enhanced when the product ability to contract in plane is restrained. (c) Experimental confirmation of enhanced wrinkle flattening for tightening product application on SILBIONE® RTV 4528 (scale bar: 200 μm); the wrinkle shape before (black) and after (red) 3.5 h of curing and cutting are also drawn for comparison. (d) Experiment ($n = 1$) *vs.* finite-element prediction for wrinkle amplitude reduction: the enhanced flattening ability of the cosmetic film is mostly captured by the presented computational model, especially if compared to the application condition that features free in-plane contraction (dashed line). (e) Schematics illustrating the mechanism that allows a contractile inextensible string to ensure 'amplitude' reductions exceeding the extent of its contraction. A limitation to the longitudinal shrinkage, here exemplified by a force imposed after contraction rather than explicitly by the substrate, requires the string shape to be modified in order to accommodate the overall length reduction caused by the contraction itself. (For interpretation of the references to colors in this figure legend, the reader is referred to the web version of this article.).

Table 3
Constitutive model parameters for tightening product action upon curing, combining an isotropic (pseudo)-thermal contraction with a hyperelastic mechanical behavior.

Coefficient	Value
α	0.0132 K^{-1}
ΔT	-6.74 K
C_{10}	-256.115 MPa
C_{01}	260.471 MPa
C_{20}	522,895 MPa
C_{11}	-1,096,750 MPa
C_{02}	575,830 MPa
D_1	0 Mpa^{-1}
D_2	0 Mpa^{-1}

film (Fig. 8c). Visualization of the wrinkle shape after 3.5 h curing showed that the amplitude was reduced by about 37% (Fig. 8c and d). Corresponding simulations assuming a film thickness of 37.5 μm (average measured dry value, range: 37-38 μm) predicted an amplitude reduction of 48% (Fig. 8d), thus confirming that the wrinkle alleviation attained in the presence of a substrate is much larger than the one corresponding to the product contracting freely, *i.e.* without a substrate (8.6% amplitude reduction, slightly larger than the 7% previously indicated as a consequence of the longer curing time: 3.5 h *vs.* 30 min). Note that, although the model prediction overestimates the experimental observation by about 30%, this is well within the range of the typical variability associated with the experiments performed to quantify the extent of product contraction and in line with the model's general tendency to overestimate such quantity (*cf.* Figs. 6b and 7a). Taken together, these results unveil the mechanisms allowing a contractile layer to induce important wrinkle alleviation, and demonstrate a direct relation between constraints to the film in-plane displacements and wrinkle amplitude reduction.

3.5. Influence of cosmetic application parameters on wrinkle alleviation

To provide additional insights into the mechanisms of wrinkle alleviation, the model of film application on a cutis with free ends (Fig. 4d) was modified in order to vary the following cosmetic application parameters: i) the film contractility, quantified by the 'target' strain, ε_{tgt}, that would be reached by a free-standing layer after 30 min curing (*cf.* Fig. 4f); ii) its deformability, measured in terms of shear modulus μ_f[‡]; iii) the thickness of the cosmetic layer; iv) the uniformity of the film thickness throughout the wrinkle profile (*i.e.* on the xz plane, *cf.* Fig. 4d); v) the deformability of the cutis, measured by the constitutive model parameter μ_0; vi) the thickness of the substrate.

3.5.1. Influence of film contractility

As visible in Fig. 9a, a more (less) contractile film led to an increase (decrease) in both the extents of periodicity and amplitude reduction. This is due to the direct relation between film contraction upon curing and wrinkle attenuation. However, the predicted changes were not directly proportional to the variation in film contractility. This is most certainly due to the mechanical non-linearity of the cutis, which directly affects the resistance opposed by substrate to the tightening action of cosmetic materials with different contractility.

[‡] The shear modulus for a 2nd order polynomial hyperelastic material is given by [38]: $\mu_f = 2(C_{10} + C_{01})$.

3.5.2. Influence of film deformability

The deformability of the cosmetic layer directly impacts its ability to dominate the mechanical balance of the substrate-film bilayer. Indeed, increasing (decreasing) the value of μ_f resulted in larger (smaller) periodicity reduction (Fig. 9b), and this contributed to reduce (enhance) the amplitude reduction, in line with the observations of Fig. 8b.

3.5.3. Influence of film thickness

Similar to the film deformability, its thickness contributes to the mechanical balance of the system. Indeed, increasing (decreasing) the value of this geometrical parameter resulted in larger (smaller) periodicity reduction (Fig. 9c), and this contributed to reduce (enhance) the amplitude reduction. However, the predicted changes in terms of amplitude reduction were not directly proportional to the thickness variations; this is most certainly due to the contribution of the film thickness to the energy required to bend the cosmetic film in order to reduce the wrinkle amplitude.

3.5.4. Influence of film thickness uniformity

In typical application conditions *in vivo*, the cosmetic film is expected to accumulate at the wrinkle valleys; its thickness will thus be larger here than at the crests. To analyze the effect of such a non-uniform cosmetic material deposition along the wrinkle profile, the film thickness at the crests and valleys was varied while maintaining the same average value ($t_f = (t_c + t_v)/2 = 60$ μm); this corresponds to applying a fixed amount of material. The results in Fig. 9d show that both the extent of periodicity and amplitude reduction are affected by the distribution of the cosmetic film. Specifically, partially filling the wrinkle valleys with the cosmetic material enhanced its effect on the wrinkle periodicity but weakened the amplitude reduction. This is most likely associated with the local increase in terms of film thickness and bending rigidity, whose role towards wrinkle alleviation has been also highlighted in Section 3.5.3. Taken together, these results indicate that the attained cosmetic effect will be sensitive to material accumulation at the wrinkle valleys.

3.5.5. Influence of cutis deformability

Similar to that of the film, the cutis deformability contributes to the mechanical balance of the system, although with an opposite role. When the model parameter μ_0 is decreased, the substrate opposes less resistance to the film action, and vice versa. As visible in Fig. 9e, larger (smaller) values of μ_0 resulted in a less (more) pronounced periodicity reduction and, correspondingly, a stronger (weaker) amplitude reduction.

3.5.6. Influence of substrate thickness

Finally, the thickness of the cutis also contributes to the film ability to dominate the substrate. Since the compressive deformation imposed by the cosmetic material is propagated throughout the substrate depth, its thickness determines the amount of material that has to be deformed in order to accommodate the film contraction. Indeed, Fig. 9f shows that increasing (decreasing) the cutis thickness negatively (positively) affected the extent of periodicity reduction, and this resulted in a larger (smaller) effect in terms of wrinkle amplitude.

4. Discussion

Cosmetic products for skin tightening have been gaining increasing attention as rapid and durable means to enhance skin firmness and mitigate surface imperfections or wrinkles. Contrary to other cosmetic treatments, these materials impose a mechani-

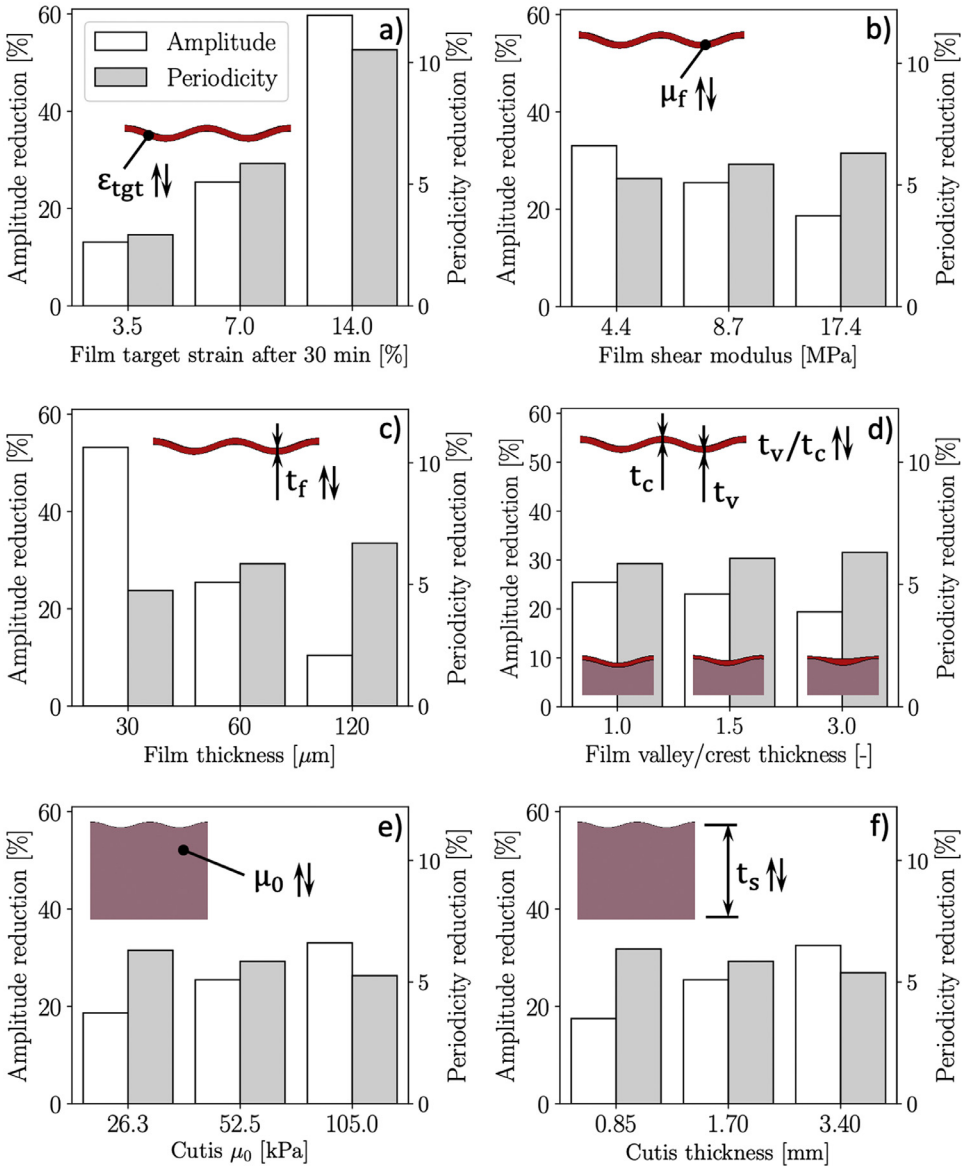

Fig. 9. *In silico* analyses of the influence of several cosmetic application parameter on the attained wrinkle-alleviating effect. (a) Role of film contractility: larger values positively affect both amplitude and periodicity reduction. (b and c) Role of film shear modulus and average thickness: larger values enhance periodicity reduction but weaken the amplitude reduction. (d) Role of cosmetic material distribution along the wrinkle profile for a film with constant average thickness (60 μm): a larger thickness at the wrinkle valleys enhances periodicity reduction but weakens amplitude reduction. (e and f) Role of the cutis characteristics: larger values of either the modeling parameter μ_0 (akin to a shear modulus) or the substrate thickness weaken the periodicity reduction but enhance amplitude reduction.

cal contraction onto the native tissue. However, their mechanical behavior is currently poorly characterized, and this limits the understanding and possible optimization of their capabilities of action. The present work aimed to explore the mechanisms underlying the cosmetic evidence of skin tightening and surface wrinkle reduction, as well as the corresponding biomechanical effects on the native tissue.

4.1. Quantitative determination of product contraction upon curing

Two dedicated experimental methods, which may be used to characterize the kinematical behavior of cosmetic products with a tightening action, were developed as part of this work. On the one hand, a very-soft, gel-like substrate (E = 6.6 kPa) was endowed with fluorescent particles that allowed the in-plane contractile action exerted by the cosmetic film to be quantified in the absence of significant outer constraints. This provided an approximation of the maximum possible extent of product contraction, corresponding to an areal strain of −13%. On the other hand, the area of the region covered by the cosmetic film was only reduced by 4.7% for a much stiffer substrate (E = 1.5 MPa), in an experimental setting akin to the one adopted in [15]. *In vivo* experiments showed that the effect obtained on skin (secant modulus at 5%: 33.3 kPa) falls in-between these two extreme conditions, reaching an areal strain of −9.6%. These results provide quantitative evidence of the product in-plane contraction upon curing, and demonstrate a dependency of its active contractile behavior on the stiffness of the substrate (Fig. 6d). Moreover, comparing the film thickness before and after 2 h of curing on SMI G/G 0.020″ revealed a 54% reduction, thus providing evidence of anisotropic product contraction. The corresponding large volume change – estimated to reach 56% – can be explained in terms of significant compound mass loss, which mainly occurs through the film thickness due to a joint effect of evaporation and substrate absorption.

4.2. Mechanisms of skin tightening

The *in vivo* measurements provided information on the extent of skin contraction and stiffening on the cheek of 24 women in a wide age range (18-71 y, *cf.* Fig. 1a). After 30 min, both the area and deformability of the film-covered tissue region were visibly reduced, indicating that the cosmetic layer was able to impose and maintain the prescribed level of tissue deformation due to its higher stiffness compared to that of the underlying skin. We reason that cosmetic products with a tightening action alter the skin resistance to deformation via two counteracting effects: i) a reduction in the tissue tangent stiffness, associated with the imposed in-plane contraction; and ii) an increased structural rigidity, due to the presence of an additional stiff surface layer; the latter was dominant for the analyzed product. The measured stiffening falls well within the range provided by Jachowicz *et al.* [13], and is in line with the expectations for application of a cosmetic layer whose Young's modulus exceeds typical values previously reported for human skin [26,29,38,39]. Conversely, Yu *et al.* [12] observed enhanced deformability after cosmetic application, which is in line with the lower Young's modulus (~500 kPa [12]) of their biomaterial. Moreover, the reversibility of tissue deformation in the 2 mm ramp-like suction protocol was greatly enhanced by the cosmetic product application, confirming the findings of Yu *et al.* [12]. This can be explained by a combination of the biomechanical behavior of the cutis with a stiffer and much less dissipative film, which directly affects the magnitude and the characteristic time scales of the deformation processes activated during the experiments. Taken together, these results clarify the mechanisms underlying skin tightening by showing that such effect is obtained via a combination of a product's kinematic, *i.e.* extent of contraction, and constitutive behavior, *i.e.* its deformability. These two parameters are thus instrumental to attaining the desired cosmetic effect and might constitute crucial targets for optimization of product formulation or application conditions.

4.3. Limitations to in-plane contraction may enhance the wrinkle-alleviating effect

Investigating the application of the tightening product on a wrinkled synthetic substrate allowed further qualifying the proposed numerical model and rationalizing the corresponding wrinkle-alleviating effect. While the product action would *per se* cause an amplitude reduction slightly below 10%, experiments on a corrugated elastomeric substrate with skin-like deformability resulted in a significantly larger effect ($\geq$ 37%), which our model could reproduce to a good extent (Fig. 8d). We note that the mechanical nature of the film-induced wrinkle alleviation is fundamentally different from the one of wrinkle formation in a film-substrate bilayer under various loading conditions, which has been – and still is – a topic of great interest in the literature [40–42]. Contrary to such cases, the curing process reduces the dimensions of the already "wrinkled" cosmetic film, thus not activating any buckling-like instabilities.

Simulating the cosmetic product application on a wrinkled cutis confirmed the enhanced flattening action as compared to the freely contracting case (Fig. 8a), with amplitude reductions ranging from 25.5% (no outer constraints to the tissue in-plane contraction) up to 79.1% (contraction fully impeded). Experimental values of imperfection reduction *in vivo* have been provided by Yu *et al.* [12], who observed up to 50% reduction after 1-4 h of cosmetic application; this value falls well within the range of the limiting cases simulated here. Our results thus identify a direct correlation between limitations to a cosmetic product's in-plane contraction and enhancement of its wrinkle reduction effect. This phenomenon can be readily understood by analogy with the case of a loose and inextensible string (Fig. 8e), which is first shrunk isotropically (from grey to black dashed curve, this transition being representative of the film curing) and then pulled in order to recover the original length of the string projection along the pulling direction (from dashed to solid curve; the applied force provides a simplified representation of the resistance opposed by the substrate or by external boundary conditions, such as in Fig. 4e). This is only possible at the expenses of a reduction in the string curvature, and thus the amplitude of its corrugation.

Contrary to this simplified model, the effective wrinkle amplitude reduction *in vivo* will be determined by a number of factors, some of which have been addressed in Section 3.5. Specifically, we showed that the attained amplitude reduction is intimately related to the balance between the contractile action of the film and the resistance opposed by the substrate. While the former is enhanced by a stronger cosmetic material contractility – determined by the chemical processes driving the volume change upon curing – and by thicker and less deformable films, the substrate resistance is determined by the deformability and thickness of the skin. For all the parametric variations considered here, a larger final periodicity corresponded to a stronger wrinkle amplitude reduction, in line with the mechanism illustrated in Fig. 8e. Note that the present investigation of potential factors influencing the cosmetic efficacy of tightening product is far from being exhaustive and does not address the possible interplay among several parameters. Furthermore, we expect the following design and application factors to also have an important effect: i) the film's and the substrate's inelastic, anisotropic, and time-dependent characteristics; ii) the presence of *in vivo* pre-tension in skin; iii) the adhesion between the film and the substrate; and iv) the wrinkle aspect ratio, determining the geometrical relationship between limitations to longitudinal contraction and corresponding wrinkle amplitude reduction. In fact, skin deformability will be relevant not only towards the film ability to contract in plane, which we showed to be more strongly limited for less deformable skins, but also towards the deformation energy required for wrinkle alleviation, which will be lower for more deformable substrates. This suggests that the cosmetic effect of tightening products may be optimized according to the substrate mechanical characteristics, and the optimal outcome on skin will be possibly affected by a combination of its anisotropic tensile and compressive properties. Notably, a thorough characterization of the multiple factors influencing the extent of skin tightening via cosmetic products might have far-reaching implications, including clinically-relevant ones. Indeed, imposing a specific state of deformation in skin regions of interest might be the key to non-invasively triggering mechanobiological pathways of tissue remodeling. Besides cosmetics, this would be applicable to, *e.g.*, controlling the mechanical environment of a wound, a factor that has been shown to affect the outcome of the healing process [43,44]. In a similar context, the contractile action of tightening cosmetic materials, combined with a suitable measurement technique, may enable quantifying the mechanical heterogeneity of skin regions featuring healing wounds [45] or other types of lesions [46,47].

4.4. Numerical model of the passive and active behavior of the tightening product

The presented data on the contractile and constitutive behavior of the analyzed tightening product provided the basis to develop a numerical model able to describe its action. Among several available models for the contraction of a film when deposited on a substrate (*e.g.* [48,49]), we chose to follow a pseudo-thermal approach similar to the one of [50]. This relates the stress induced by the film curing to a geometrical change, which is induced by a field variable akin to a temperature and can be represented using

a framework that is readily available in most commercial finite-element packages. Despite the relatively simple formulation, which neglects the gradual film stiffening as well as the significant mass loss that occurs during curing, our model was able to capture all relevant features of the processes observed *in vivo* and *in vitro*. Specifically, skin tightening was represented quite well, both in terms of area contraction and overall mechanical response (Fig. 7), thus making the developed model well-suited to test the mechanisms of interaction between tightening products and substrates, as was done in Sections 3.4 and 3.5 for application on corrugated substrates. While accurate quantification of the role of each parameter affecting skin characteristics will require a dedicated and separate study, our numerical model is also particularly relevant towards product design optimization, *e.g.* by allowing the influence of film contraction and stiffness to be investigated separately, or by enabling comparison of alternative application conditions, *e.g.* layer geometries. In this context, a computational framework might significantly speed up the exploration of the parameter space and the identification of potentially optimal settings to be verified experimentally.

4.5. Limitations and future work

Our study also features a few limitations, which should be addressed and may suggest avenues for future development. First, the experimental characterization of the action of the cosmetic product on skin was limited to relatively short time periods (30 min), whereas the longer-term behavior was determined exclusively *in vitro*. While preservation of the mechanical effects over time is certainly crucial to ensure durability of the cosmetic outcome, it should be noted that rigorous quantifications of the tightening product action *in vivo* over a long period of time is rather delicate in terms of subjects' comfort, which directly affects the quality of the measurements. Moreover, the curing of the product appeared to be faster *in vivo* than on synthetic substrates, possibly due to enhanced absorption properties of the skin, so that the evolution of the film characteristics appeared as practically complete after 25-30 min.

Second, the final value of film thickness in skin applications was estimated and not directly measured. While this most certainly influences the simulation results reported in Fig. 7, we note that destructive separation of the film from the underlying skin might result in irremediable alterations of its characteristics, thus not providing additional information. Future work should consider *in situ* quantification of the cosmetic layer thickness throughout curing, for instance by use of non-invasive optical techniques.

Third, the substrates used for the *in vitro* experiments do not fully capture the complexity of the skin biomechanical behavior, such as its anisotropy and the presence of pre-tension. Future analyses should most definitely account for the direction-dependent cosmetic effect that tightening products might yield *in vivo*. In fact, comparing the extent of film contraction along several directions may even provide an easy approach to quantifying skin anisotropy, which is typically overlooked by suction-based measurement procedures. Moreover, the corrugated elastomeric substrates feature wrinkles in a stress-free state, while the occurrence of wrinkles in skin is often associated with the presence of internal stresses [51]. We also note that soft materials with graded stiffness, such as the skin, may not only form wrinkles, but also creases and folds [52–55], and tightening cosmetic products might be used to reduce the visibility of such imperfections. Our computational framework might provide a means to address the role of these additional complexities and application conditions *in silico*, although corresponding experimental verifications are certainly needed in order to draw meaningful conclusions on the expected cosmetic outcomes.

Additional limitations are provided by the modeling assumptions. The large thickness (and volume) reductions of the cosmetic product were not explicitly represented, relying on the final film thickness values; the thickness reduction should be analyzed through a dedicated set of *in vitro* and *in vivo* experiments, eventually allowing the proposed computational framework to be refined. Representation of the product mechanical behavior was also strongly simplified in the model, as this was assumed to behave hyperelastically and to stiffen instantaneously rather than gradually. Despite not directly affecting any of the results presented here, both assumptions appear to be quite unrealistic and should be addressed in improved model formulations that aim to accurately predict cosmetic effects.

Finally, investigation of the product action on wrinkled substrates was mainly aimed at explaining the enhanced amplitude reduction with respect to the freely contracting case. Future work shall first corroborate the experimental validation of our model predictions by combining *in vitro* and *in vivo* measurements, and then address the role of the several factors influencing the cosmetic effect and its durability. While these investigations clearly exceed the scope of the present work, use of the proposed computational framework will greatly facilitate testing of alternative conditions and identification of optimal parameter combinations, thus providing fundamental aid towards rational product design and application.

5. Conclusions

The mechanical characteristics of a soft active biomaterial for skin anti-aging were assessed considering a wide range of experimental conditions, providing the data required to inform a numerical model of the attained cosmetic action. The corresponding *in vivo* effects on the tissue biomechanics were rationalized by considering the combined role of the film stiffness and of its contractile action, as well as their interplay with the substrate mechanical behavior. Moreover, wrinkle alleviation was shown to be greatly enhanced by a substrate with skin-like deformability, due to the corresponding limitations to the film contraction in plane. Finally, the developed numerical model was used for parametric studies providing insights that are relevant for optimization of this fascinating class of biomaterials.

Disclosures

This work was conducted in the framework of a collaboration between ETH Zurich and L'Oréal Research & Innovation. Some of the authors are currently employed by L'Oréal Research & Innovation.

Statement of significance

Commercial interest for cosmetic products with tightening action is on the rise, due to their anti-aging effect through mechanical smoothing of the skin. Despite growing evidence on their ability to modulate the native tissue's biomechanics and morphology, the mechanics of these biomaterials and the mechanisms regulating interaction with the underlying tissue are poorly characterized and only partially understood. We present a wide-range investigation of one product's action on several substrates, demonstrating an important role of the ratio between the stiffness of the substrate and that of the cosmetic film towards maximizing the attained tightening effect. We further derive a corresponding computational model, which we envision to impact further development, optimization, and exploitation of this fascinating class of soft active biomaterials.

Declaration of Competing Interest

This work was conducted in the framework of a collaboration between ETH Zurich and L'Oréal Research & Innovation, which involved funding from L'Oréal Research & Innovation. The analyzed cosmetic product is developed by L'Oréal Research & Innovation and was provided to ETH Zurich as part of this scientific collaboration. Some of the authors are currently employed by L'Oréal Research & Innovation.

Acknowledgements

The authors wish to thank Laura Bernardi, Anna Moro, and Xi Wu from the Institute for Mechanical Systems (IMES) of ETH Zurich for their invaluable help in setting up the experimental protocols, as well as the group of Prof. Jürg Dual (IMES, ETH Zurich) for the use of the white light interferometer. We also wish to thank Alexandra Farran, Anne-Laure Bernard (L'Oréal USA), Pierre Dupuis (L'Oréal France) and Florian Formanek (HORIBA Scientific) for useful discussions, Hussein Jouni (L'Oréal France) for his help with the statistical analysis, and Audrey Gueniche (L'Oréal France) for critical reading of the manuscript. This work was partially supported by L'Oréal Research & Innovation in the framework of a scientific collaboration with ETH Zurich.

Supplementary materials

Supplementary material associated with this article can be found, in the online version, at doi:10.1016/j.actbio.2020.08.027.

References

[1] E. Makrantonaki, C.C. Zouboulis, Molecular mechanisms of skin aging: state of the art, Ann. N. Y. Acad. Sci. 1119 (2007) 40–50, doi:10.1196/annals.1404.027.
[2] C. Longo, A. Casari, F. Beretti, A.M. Cesinaro, G. Pellacani, Skin aging: in vivo microscopic assessment of epidermal and dermal changes by means of confocal microscopy, J. Am. Acad. Dermatol. 68 (2013) e73–e82, doi:10.1016/j.jaad.2011.08.021.
[3] J.L. Contet-Audonneau, C. Jeanmaire, G. Pauly, A histological study of human wrinkle structures: comparison between sun-exposed areas of the face, with or without wrinkles, and sun-protected areas, Br. J. Dermatol. 140 (1999) 1038–1047, doi:10.1046/j.1365-2133.1999.02901.x.
[4] E.F. Bernstein, Yue Qiu Chen, J.B. Kopp, L. Fisher, D.B. Brown, P.J. Hahn, F.A. Robey, J. Lakkakorpi, J. Uitto, Long-term sun exposure alters the collagen of the papillary dermis: comparison of sun-protected and photoaged skin by Northern analysis immunohistochemical staining, and confocal laser scanning microscopy, J. Am. Acad. Dermatol. 34 (1996) 209–218, doi:10.1016/S0190-9622(96)80114-9.
[5] C. Griffiths, A.N. Russman, G. Majmudar, R.S. Singer, T.A. Hamilton, J.J. Voorhees, Restoration of collagen formation in photodamaged human skin by tretinoin (retinoic acid), N. Engl. J. Med. 329 (1993) 530–535, doi:10.1056/NEJM199308193290803.
[6] E. Makrantonaki, C.C. Zouboulis, Characteristics and pathomechanisms of endogenously aged skin, Dermatology 214 (2007) 352–360, doi:10.1159/000100890.
[7] J. Varani, D. Spearman, P. Perone, S.E.G. Fligiel, S.C. Datta, Z.Q. Wang, Y. Shao, S. Kang, G.J. Fisher, J.J. Voorhees, Inhibition of type I procollagen synthesis by damaged collagen in photoaged skin and by collagenase-degraded collagen in vitro, Am. J. Pathol. 158 (2001) 931–942, doi:10.1016/S0002-9440(10)64040-0.
[8] J. Uitto, Connective tissue biochemistry of the aging dermis. Age-related alterations in collagen and elastin, Dermatol. Clin. 4 (1986) 433–446, doi:10.1016/S0733-8635(18)30806-4.
[9] A. Nebel, P.J.P. Croucher, R. Stiegeler, S. Nikolaus, M. Krawczak, S. Schreiber, No association between microsomal triglyceride transfer protein (MTP) haplotype and longevity in humans, in: Proceedings of the National Academy of Sciences of the United States of America, 102, 2005, pp. 7906–7909, doi:10.1073/pnas.0408670102.
[10] S. Diridollou, V. Vabre, M. Berson, L. Vaillant, D. Black, J.M. Lagarde, J.M. Grégoire, Y. Gall, F. Patat, Skin ageing: changes of physical properties of human skin in vivo, Int. J. Cosmet. Sci. 23 (2001) 353–362, doi:10.1046/j.0412-5463.2001.00105.x.
[11] B.A. Gilchrest, Skin aging and photoaging: an overview, J. Am. Acad. Dermatol. 21 (1989) 610–613, doi:10.1016/S0190-9622(89)70227-9.
[12] B. Yu, S.Y. Kang, A. Akthakul, N. Ramadurai, M. Pilkenton, A. Patel, A. Nashat, D.G. Anderson, F.H. Sakamoto, B.A. Gilchrest, R.R. Anderson, R. Langer, An elastic second skin, Nat. Mater. 15 (2016) 911–918, doi:10.1038/nmat4635.
[13] J. Jachowicz, R. Mcmullen, D. Prettypaul, Alteration of skin mechanics by thin polymer films, Skin Res. Technol. 14 (2008) 312–319, doi:10.1111/j.1600-0846.2008.00296.x.
[14] M.N.G. de Mul, T. Uddin, X. Yan, A. Hubschmitt, B. Klotz, W.K.M. Chan, Reducing facial wrinkle size and increasing skin firmness using skin care polym, J. Cosmet. Sci. 69 (2018) 131–143.
[15] R. Maidhof, E. Knapp, F. Liebel, M. Fair, E.H. Rubinson, Technical approaches to select high-performance instant skin smoothing formulations: correlation of in vitro and in vivo assessment methods, Skin Res. Technol. (2019), doi:10.1111/srt.12691.
[16] C. Fox, Skin tightening formulation and method for treating skin, U.S. Patent No. 5,879,684 A (1999).
[17] H. Delage-Grouiller, B. Noe, C. Mahe, Cosmetic composition with skin tightening effect, U.S. Patent No. 8,986,667 B2 (2015).
[18] L.E. Manning, M. Wang, A.A. Galdi, C. Chiou, Skin tightening compositions, U.S. Patent No. 9,770,401 B2 (2017).
[19] E. Cerda, L. Mahadevan, Geometry and physics of wrinkling, Phys. Rev. Lett. 90 (2003) 4, doi:10.1103/PhysRevLett.90.074302.
[20] S. Budday, P. Steinmann, E. Kuhl, The role of mechanics during brain development, J. Mech. Phys. Solids 72 (2014) 75–92, doi:10.1016/j.jmps.2014.07.010.
[21] C.M. Chen, S. Yang, Wrinkling instabilities in polymer films and their applications, Polym. Int. 61 (2012) 1041–1047, doi:10.1002/pi.4223.
[22] Y. Zhao, B. Feng, J. Lee, N. Lu, D.M. Pierce, A multi-layered model of human skin elucidates mechanisms of wrinkling in the forehead, J. Mech. Behav. Biomed. Mater. (2020) 105, doi:10.1016/j.jmbbm.2020.103694.
[23] World Medical Association declaration of Helsinki, Ethical principles for medical research involving human subjects, JAMA - J. Am. Med. Assoc. 310 (2013) 2191–2194, doi:10.1001/jama.2013.281053.
[24] International Council for Harmonisation of Technical Requirements for Pharmaceuticals for Human Use, E6 (R2): Guideline for good clinical practice - Step 5, European Medicines Agency (2016). https://www.ema.europa.eu/en/ich-e6-r2-good-clinical-practice.
[25] R. Hopf, L. Bernardi, J. Menze, M. Zündel, E. Mazza, A.E. Ehret, Experimental and theoretical analyses of the age-dependent large-strain behavior of Sylgard 184 (10:1) silicone elastomer, J. Mech. Behav. Biomed. Mater. 60 (2016) 425–437, doi:10.1016/j.jmbbm.2016.02.022.
[26] J. Weickenmeier, M. Jabareen, E. Mazza, Suction based mechanical characterization of superficial facial soft tissues, J. Biomech. 48 (2015) 4279–4286, doi:10.1016/j.jbiomech.2015.10.039.
[27] M. Pensalfini, J. Weickenmeier, M. Rominger, R. Santoprete, O. Distler, E. Mazza, Location-specific mechanical response and morphology of facial soft tissues, J. Mech. Behav. Biomed. Mater. 78 (2018) 108–115, doi:10.1016/j.jmbbm.2017.10.021.
[28] L. Bernardi, R. Hopf, A. Ferrari, A.E. Ehret, E. Mazza, On the large strain deformation behavior of silicone-based elastomers for biomedical applications, Polym. Test. 58 (2017) 189–198, doi:10.1016/j.polymertesting.2016.12.029.
[29] A. Wahlsten, M. Pensalfini, A. Stracuzzi, G. Restivo, R. Hopf, E. Mazza, On the compressibility and poroelasticity of human and murine skin, Biomech. Model. Mechanobiol. 18 (2019) 1079–1093, doi:10.1007/s10237-019-01129-1.
[30] X. Liang, S.A. Boppart, Biomechanical properties of in vivo human skin from dynamic optical coherence elastography, IEEE Trans. Biomed. Eng. (2010), doi:10.1109/TBME.2009.2033464.
[31] M. Pensalfini, E. Haertel, R. Hopf, M. Wietecha, S. Werner, E. Mazza, The mechanical fingerprint of murine excisional wounds, Acta Biomater. 65 (2018) 226–236, doi:10.1016/j.actbio.2017.10.021.
[32] I. Arganda-Carreras, V. Kaynig, C. Rueden, K.W. Eliceiri, J. Schindelin, A. Cardona, H.S. Seung, Trainable weka segmentation: a machine learning tool for microscopy pixel classification, Bioinformatics 33 (2017) 2424–2426, doi:10.1093/bioinformatics/btx180.
[33] C.A. Schneider, W.S. Rasband, K.W. Eliceiri, NIH Image to ImageJ: 25 years of image analysis, Nat. Methods 9 (2012) 671–675, doi:10.1038/nmeth.2089.
[34] M.B. Rubin, S.R. Bodner, A three-dimensional nonlinear model for dissipative response of soft tissue, Int. J. Solids Struct. 39 (2002) 5081–5099, doi:10.1016/S0020-7683(02)00237-8.
[35] J. Weickenmeier, M. Jabareen, Elastic-viscoplastic modeling of soft biological tissues using a mixed finite element formulation based on the relative deformation gradient, Int. J. Numer. Methods Biomed. Eng. 30 (2014) 1238–1262, doi:10.1002/cnm.2654.
[36] M. Bergert, T. Lendenmann, M. Zündel, A.E. Ehret, D. Panozzo, P. Richner, D.K. Kim, S.J.P. Kress, D.J. Norris, O. Sorkine-Hornung, E. Mazza, D. Poulikakos, A. Ferrari, Confocal reference free traction force microscopy, Nat. Commun. (2016) 7, doi:10.1038/ncomms12814.
[37] Simulia Dassault Systèmes, Abaqus 6.14, Abaqus 6.14 Analysis User's Guide. (2014).
[38] Y. Har-Shai, S.R. Bodner, D. Egozy-Golan, E.S. Lindenbaum, O. Ben-Izhak, V. Mitz, B. Hirshowitz, Viscoelastic properties of the superficial musculoaponeurotic system (SMAS): a microscopic and mechanical study, Aesthetic Plast. Surg. 21 (1997) 219–224, doi:10.1007/s002669900113.
[39] D.L. Bader, P. Bowker, Mechanical characteristics of skin and underlying tissues in vivo, Biomaterials 4 (1983) 305–308, doi:10.1016/0142-9612(83)90033-9.
[40] M. Biot, Bending of an infinite beam on an elastic foundation, J. Appl. Mech. (1937).
[41] Y. Cao, J.W. Hutchinson, Wrinkling phenomena in neo-Hookean film/substrate bilayers, J. Appl. Mech. Trans. ASME (2012), doi:10.1115/1.4005960.
[42] M.A. Holland, B. Li, X.Q. Feng, E. Kuhl, Instabilities of soft films on compliant substrates, J. Mech. Phys. Solids (2017), doi:10.1016/j.jmps.2016.09.012.

[43] S. Aarabi, K.A. Bhatt, Y. Shi, J. Paterno, E.I. Chang, S.A. Loh, J.W. Holmes, M.T. Longaker, H. Yee, G.C. Gurtner, Mechanical load initiates hypertrophic scar formation through decreased cellular apoptosis, FASEB J. (2007), doi:10.1096/fj.07-8218com.
[44] V.W. Wong, M.T. Longaker, G.C. Gurtner, Soft tissue mechanotransduction in wound healing and fibrosis, Semin. Cell Dev. Biol. (2012), doi:10.1016/j.semcdb.2012.09.010.
[45] M. Wietecha, M. Pensalfini, M. Cangkrama, B. Müller, J. Jin, J. Brinckmann, E. Mazza, S. Werner, Activin-mediated alterations of the fibroblast transcriptome and matrisome control the biomechanical properties of skin wounds, Nat. Commun. 11 (2020) 1–20.
[46] Y. Zhang, R.T. Brodell, E.N. Mostow, C.J. Vinyard, H. Marie, In vivo skin elastography with high-definition optical videos, Skin Res. Technol. (2009), doi:10.1111/j.1600-0846.2009.00351.x.
[47] S.J. Kirkpatrick, R.K. Wang, D.D. Duncan, M. Kulesz-Martin, K. Lee, Imaging the mechanical stiffness of skin lesions by in vivo acousto-optical elastography, Opt. Express (2006), doi:10.1364/oe.14.009770.
[48] A.F. Mertz, S. Banerjee, Y. Che, G.K. German, Y. Xu, C. Hyland, M.C. Marchetti, V. Horsley, E.R. Dufresne, Scaling of traction forces with the size of cohesive cell colonies, Phys. Rev. Lett. (2012), doi:10.1103/PhysRevLett.108.198101.
[49] G.K. German, W.C. Engl, E. Pashkovski, S. Banerjee, Y. Xu, A.F. Mertz, C. Hyland, E.R. Dufresne, Heterogeneous drying stresses in stratum corneum, Biophys. J. (2012), doi:10.1016/j.bpj.2012.04.045.
[50] C.M. Edwards, U.S. Schwarz, Force localization in contracting cell layers, Phys. Rev. Lett. (2011), doi:10.1103/PhysRevLett.107.128101.
[51] D. Pond, A.T. McBride, L.M. Davids, B.D. Reddy, G. Limbert, Microstructurally-based constitutive modelling of the skin – linking intrinsic ageing to microstructural parameters, J. Theor. Biol. (2018), doi:10.1016/j.jtbi.2018.01.014.
[52] M. Diab, T. Zhang, R. Zhao, H. Gao, K.S. Kim, Ruga mechanics of creasing: from instantaneous to setback creases, P. Roy. Soc. A-Math. Phy. (2013), doi:10.1098/rspa.2012.0753.
[53] R. Zhao, T. Zhang, M. Diab, H. Gao, K.S. Kim, The primary bilayer ruga-phase diagram I: localizations in ruga evolution, Extrem. Mech. Lett. (2015), doi:10.1016/j.eml.2015.04.006.
[54] L. Jin, A. Auguste, R.C. Hayward, Z. Suo, Bifurcation diagrams for the formation of wrinkles or creases in soft bilayers, J. Appl. Mech. Transactions ASME (2015), doi:10.1115/1.4030384.
[55] B. Li, Y.P. Cao, X.Q. Feng, H. Gao, Mechanics of morphological instabilities and surface wrinkling in soft materials: a review, Soft Matter. (2012), doi:10.1039/c2sm00011c.